Assimilation of sea surface salinities from SMOS in an Arctic coupled ocean and sea ice reanalysis

Jiping Xie[1], Roshin P. Raj[1], Laurent Bertino[1], Justino Martínez[2], Carolina Gabarró[2,3], and Rafael Catany[4]

[1] Nansen Environmental and Remote Sensing Center and Bjerknes Centre for Climate Research, Bergen, Norway

[2] Institute of Marine Sciences, ICM-CSIC, Barcelona, Spain

[3] Barcelona Expert Center, Barcelona, Spain

[4] ARGANS, Plymouth, UK

Corresponding author: Jiping Xie, jiping.xie@nersc.no

1 **Abstract**

2 In the Arctic, the Sea Surface Salinity (SSS) plays a key role in processes related to

3 water mixing and sea ice. However, the lack of salinity observations causes large

4 uncertainties in Arctic Ocean forecasts and reanalysis. Recently the Soil Moisture and Ocean

5 Salinity (SMOS) satellite mission was used by the Barcelona Expert Centre to develop an

6 Arctic SSS product. In this study, we evaluate the impact of assimilating this data in a

7 coupled ocean-ice data assimilation system. Using the Deterministic Ensemble Kalman filter

8 from July to December 2016, two assimilation runs respectively assimilated two successive

9 versions of the SMOS SSS product, on top of a pre-existing reanalysis run. The runs were

10 validated against independent in-situ salinity profiles in the Arctic. The results show that the

11 biases and the Root Mean Squared Differences (RMSD) of SSS are reduced by 10% to 50%

12 depending on the area, and highlight the importance of assimilating satellite salinity

13 data. The time series of Freshwater Content (FWC) further shows that its seasonal cycle can

14 be adjusted by assimilation of the SSS products, which is encouraging to assimilate SSS in a

15 long-time reanalysis to better reproduce the Arctic water cycle.

17 **Keywords**: Arctic Ocean; Sea Surface Salinity; FWC; SMOS;

1. Introduction

The Arctic Ocean is undergoing a dramatic warming, resulting in the loss of sea ice documented by previous studies (e.g., Johannessen et al., 1999; Stroeve and Notz, 2018). Sea ice melt contributes freshwater to the Arctic Ocean, together with precipitation and river flux, and has far-reaching effects on the Arctic Ocean environment (Carmack et al., 2016). The Arctic observing system, compared to other oceans, lacks the capability to provide a complete picture of ocean salinity, particularly because of obstruction by sea ice. A complete reconstruction of Arctic environmental variables thus requires a data assimilative numerical model capable of propagating information below sea ice during the winter as practiced by ocean operational forecast systems (such as Dombrowsky, 2009; Fujii et al., 2019). As with other ocean data assimilation (DA) applications, Arctic reanalysis products of ocean and sea ice play an important role in understanding climate change and its mechanisms. In recent years, many studies (e.g., Storto et al., 2019; Uotila et al., 2019) evaluated the quality of the Arctic reanalysis products and recommended experiments to maximize the usefulness of new observations, as done by Kaminski et al. (2015) and Xie et al. (2018). However, there are no impact studies of salinity observations in the Arctic to our knowledge.

Ocean salinity has been used to study the water cycle for the last 20 years (e.g., Curry et al., 2003; Boyer et al., 2005; Yu, 2011; Yu et al., 2017). A recent review paper showed a stabilization of the Freshwater Content (FWC) in the Arctic Basin, although observations indicate that the Beaufort Gyre keeps getting fresher (Solomon et al., 2021). Salinity variations have far-reaching implications for ocean mixing, water mass formation, and ocean general circulation, but suffer from large uncertainties in the Arctic, mainly due to sparse observations and the lack of a steady-state reference time period (e.g., Stroh et al., 2015; Xie et al., 2019). Measuring Sea Surface Salinity (SSS) from passive microwave remote sensing is a comparatively new but promising way to reduce the uncertainty in salinity. Launched in November 2009, the Microwave Imaging Radiometer using Aperture Synthesis (MIRAS) instrument of the European Space Agency's (ESA) Soil Moisture and Ocean Salinity (SMOS) mission measures the brightness temperatures (T_B) of the sea surface at different frequency bins. The passive 2-D interferometric radiometer on the satellite operating in L-band (1.4 GHz) is sensitive to water salinity and sufficiently free from electromagnetic interference (e.g., Font et al., 2010; Kerr et al., 2010). Since May 2010, SMOS operationally provides SSS records over the global ocean (Mecklenburg et al., 2012). During the last 12 years, large improvements have been introduced in the SMOS data processing chain, increasing the accuracy and coverage of the salinity data up to levels that were unthinkable at the beginning of the mission (Martin-Neira et al. 2016, Olmedo et al., 2018; Reul et al., 2020; Boutin et al., 2022).

54 Furthermore, the assimilation of satellite-derived SSS products using an ensemble DA

55 method has been found to significantly improve the surface and subsurface salinity fields in

56 the tropics (Lu et al. 2016). The advantages of assimilating three SSS products from SMOS,

57 Aquarius (ref., Lee et al, 2012), and the Soil Moisture Active Passive Mission (SMAP; e.g.,

58 Tang et al., 2017) into a global ocean forecast system using a 3D-Var DA method have also

59 been demonstrated by Martin et al (2019). Their results show the benefits of assimilating

60 both the SMOS and SMAP datasets in the intertropical convergence zone in the tropical

61 Pacific. However, very few studies have investigated the impact of assimilating SSS products

62 in the Arctic or high latitudes. Since the beginning, the SSS retrieval from SMOS in cold

63 regions has been very challenging for three main reasons: i) the lower sensitivity of T_B to

64 salinity in cold waters leads to larger errors (Yueh et al., 2001; e.g, the sensitivity drops from

65 0.5 to 0.3 K PSU^{-1} when sea surface temperature decreases from 15 to 5°C); ii) land-sea

66 and ice-sea contaminations resulting from abrupt changes of T_B values across these two

67 interfaces, combined with the large ground footprint of SMOS; iii) the requirement of a well-

68 observed steady-state period for the removal of biases. Addressing these challenges in the

69 SMOS salinity retrieval approach, Olmedo et al. (2017) introduced a non-Bayesian retrieval

70 method to de-bias the Level 1 baseline (L1B) salinity against the reference SSS from Argo

71 data (Argo, 2022). Level 1 data from the satellite is available within 24 hours, but the

72 additional processing steps require high-quality auxiliary data so Level 3 and 4 SSS are only

73 provided in delayed mode. Starting with the ESA L1B (v620) product from SMOS, the

74 Barcelona Expert Centre (BEC) released Version 2.0 of the Arctic gridded SSS product (25

75 km resolution; Olmedo et al., 2018). Xie et al. (2019) evaluated the V2.0 SSS product and

76 another gridded Arctic SMOS SSS product developed by LOCEAN (Boutin et al., 2018)

77 during the years 2011-2013. These two SSS observation sets, together with an Arctic

78 reanalysis (Xie et al., 2017) and one objective analysis product (Greiner et al. (2021)

79 describe an updated version of this product), were validated against in-situ observations and

80 compared with two climatology datasets: the World Ocean Atlas of 2013 (WOA2013, Zweng

81 et al., 2013) and the Polar science center Hydrographic Climatology (PHC 3.0, Steele et al.,

82 2001). They found considerable discrepancies among the different gridded SSS products,

83 especially in the freshest seawater (<24 psu). The intercomparison of these Arctic SSS

84 products shows room for improvement of the SMOS-based SSS in the Arctic.

85 Recently, under the framework of the ESA project Arctic+Salinity (AO/1-9158/18/I-BG), and

86 further development of the non-Bayesian scheme (Olmedo et al., 2017), the effective

87 resolution of SSS data was enhanced both in space and time (Martínez et al., 2022). The

88 new version of the SSS product (V3.1) has the capability to monitor mesoscale structures

89 and river discharges (e.g., Martínez et al., 2022). This new product provides daily maps

90 (Level 4) of 9-day averages in the Arctic on a regular 25 km grid and covers a longer time

91 period 2011-2019, and are released through the BEC portal (http://bec.icm.csic.es/ and also

92 at DOI: 10.20350/digitalCSIC/12620; last accessed May 2022). The major differences in the

93 estimation of the two SSS products (V2.0 and V3.1) are detailed in the Algorithm Theoretical

94 Baseline Document (ATBD) of the Arctic+Salinity project (Martínez et al., 2020). Figure 1

95 shows that in comparison to V2.0, V3.1 provides wider coverage in the marginal seas around

96 the Arctic and is also fresher as indicated by the 26 psu isoline.

97 The two successive versions of the BEC SMOS SSS products are assimilated into the

98 TOPAZ Arctic reanalysis system (detailed in Section 2) during the summer of 2016. These

99 two assimilation runs are compared to the Arctic reanalysis without assimilation of satellite

100 SSS data which is identical to the product ARCTIC_REANALYSIS_PHYS_002_003 in the

101 Copernicus Marine Services. The model validation against independent observations

102 presents the differences stemming from these two SSS products, although they are from the

103 same initial data source (SMOS). Their impact on the assimilation in the Arctic coupled ice-

104 ocean model shows large differences, thereby motivating further efforts to improve SSS

105 retrievals in the cold Arctic.

106 The paper is organized as follows: Section 2 briefly describes the coupled ocean and sea ice

107 data assimilation system and the assimilation experiments; Section 3 describes the in-situ

108 observations and the validation metrics; results presented in Section 4 include the validation

109 using independent SSS observations, separated into different ocean basins. Section 4 also

110 examines the impact of SSS assimilation on the weekly increments of other related variables

111 near the surface, and explores the integrated effect on the freshwater simulated by the

112 model. In Section 5, the findings of this study and future perspectives are summarized.

113

114 **2. Assimilation system and experimental design**

115 *2.1 The Arctic ocean and sea-ice coupled data assimilation system*

116 TOPAZ is a coupled ocean and sea ice data assimilation system, built using the

117 Deterministic Ensemble Kalman Filter (DEnKF; Sakov et al., 2012) to simultaneously

118 assimilate multiple types of observations for the ocean and sea ice (Xie et al., 2017). The

119 ocean model in this system uses version 2.2 of the Hybrid Coordinate Ocean Model

120 (HYCOM; Chassignet et al., 2003) with a low-distortion square grid at a horizontal resolution

121 of 12-16 km. The river discharge input is climatological, using the ERA-Interim (Dee et al.,

122 2011) runoffs channeled in a simple hydrological model, which tends to underestimate the

123 amplitude of the seasonal cycle and thus produces a saline bias at the surface (Xie et al.

124 2019). The coupled sea ice model uses a single-category thermodynamic model (Drange

125   and Simonsen, 1996) and dynamics by the modified elastic-viscous-plastic rheology

126   (Bouillon et al., 2013) from an early version of the CICE model (Lisæter et al. 2003). The

127   model covers the Arctic Ocean and the whole north Atlantic Ocean (shown in Fig. 1 in Xie et

128   al., 2017). A seasonal inflow of Pacific Water is imposed across the Bering Strait, based on

129   observed transports (Woodgate et al., 2012). At all lateral boundaries, the temperature and

130   salinity stratifications are relaxed to a climatology combining version 2.0 of WOA2013 and

131   version 3.0 of PHC with a 20-grid cells buffer zone. To avoid a potential model drift, the

132   surface salinity is relaxed to the combined climatology as mentioned above, with a 30-day

133   timescale, but the relaxation is suppressed wherever the difference from climatology exceeds

134   0.5 psu to avoid the artificial formation of bulk surface freshwater layers.

135   For simplification, the two steps of the assimilation system can be translated by the

136   following concept expressions (update and model propagation):

137   $$\mathbf{X}_a = \mathbf{X}_f + \mathbf{K}(\mathbf{y} - H\mathbf{X}_f) \qquad (1)$$

138   $$\mathbf{X}_f = M(\mathbf{X}_a) \qquad (2)$$

139   Where the matrix **X** represents the model state with all 3-D and 2-D variables needed by

140   the model forward integration, represented by the operator M. The subscripts 'a' and 'f'

141   respectively indicate the analyzed model state obtained through optimization after DA and

142   the model forecast. The vector **y** is composed of the quality-checked observations during the

143   weekly cycle, and the observation operator H gives the model equivalent of the observations.

144   The innovation term (in parentheses in Eq.1) represents the differences between the model

145   and the various observations in the observation space.

146   For the ensemble data assimilation method, the matrix **X** includes the dynamical members

147   of the model states as different columns and further evolutes according to Eqs. 1 and 2 as

148   described in the DEnKF. The TOPAZ model runs an ensemble of 100 members. The **K**

149   matrix (Kalman gain) is calculated using the ensemble covariance matrix. Like other square

150   root versions of the Ensemble Kalman Filter, the DEnKF splits Eq. 1 into two steps: the **K**

151   calculation is applied to the ensemble mean, and the anomalies are updated to match a

152   target analysis covariance (more details in Sakov et al., 2012). Using a 7-day assimilation

153   cycle, we use the DEnKF to assimilate different types of ocean and ice observations,

154   including along-track sea level anomaly (SLA), sea surface temperature (SST), in-situ

155   profiles of temperature and salinity, sea ice concentrations (SIC) and sea ice drift products all

156   sourced from the Copernicus Marine Environment Monitoring Services (CMEMS;

157   https://marine.copernicus.eu). The same TOPAZ system provides a 10-day forecast of ocean

158   physics and biogeochemistry in the Arctic (Bertino et al., 2021) every day via the CMEMS

159   portal.

160

2.2 Assimilation experiments and the observation error estimate for SSS

To evaluate the impact of the assimilation of two versions of the SSS products on TOPAZ model runs, a control assimilation experiment (Exp0) and two parallel assimilation experiments (ExpV2, ExpV3) for a 6-month time period (July to December 2016) were performed. Exp0 assimilates all available ocean and sea ice data, except the satellite SSS products. On the other hand, ExpV2 and ExpV3 additionally assimilate the BEC SSS products V2.0 and V3.1, respectively. Details of the three assimilation runs are listed in Table 1.

Observation error is a key parameter in any DA system: too small values lead to overfitting, while too large values make the assimilation inefficient. The salinity errors from passive microwave instruments were previously estimated by Vinogradova et al. (2014): the zonal average of standard errors north of 60°N was estimated at 0.6 psu. In a recent study, Xie et al. (2019) evaluated the SMOS-based SSS products using in-situ observations and revealed strong regional dependence for the V2.0 product errors: smaller than 0.4 psu in the Northern Atlantic but increasing dramatically to 1 psu in the Nordic seas and over 2 psu in the central Arctic. Undoubtedly, the salinity observation errors from passive microwave instruments are higher in high latitudes than elsewhere. Furthermore, in the Beaufort Sea (as Fig. 12a in Xie et al., 2019), the error of the SSS V2.0 product and the Arctic reanalysis product from TOPAZ (same as Exp0 used in this study) both show an inverse relationship between SSS values and SSS errors. Hence, we use an empirical error function for ExpV2 and ExpV3 adjusted to the discrepancies as shown in Eq. 3, following Xie et al. (2019):

$$E_{SSS} = max\left\{E_{int}, \left[0.6 + \frac{6}{1+exp\left(\frac{SSS-16}{5}\right)}\right]^2\right\} \tag{3}$$

Where E_{int} is the instrumental error variance estimated by the data provider, that part is absent from the V2.0 product. Eq. 3 yields more conservative error estimates than the providers, which also prevents the discontinuities caused by strong assimilation updates (as an example noticed by Balibrea-Iniesta et al., 2018). The settings for all other observation types are identical to those applied in Xie et al. (2017). By construction, the observation errors are always larger for the V3.1 than the V2.0 product, but in fresh waters they are identical. This implies that the assimilation may pull the analysis closer to the V2.0 than the V3.1 product in the more saline waters, but they are otherwise treated on equal footing, ignoring the a priori expectation that the most recent product should be more reliable.

3. In-situ SSS observations for validation

194   All in-situ salinity profiles were collected from various repositories and cruises (as shown in

195   Fig. 2). Salinity measurements were extracted near the surface over the Arctic domain during

196   the experimental time period. The sanity check procedures include: i) location check to

197   remove SSS observations in the model land mask; ii) omit the invalid profiles if the top depth

198   is deeper than 8 m; iii) remove redundant observations. Since the model does not reproduce

199   local gradients of the vertical salinity profiles shown in Supply et al. (2020), all the salinity

200   profiles are averaged over the upper 8 meters below the surface. This also avoids the loss of

201   the profiles that do not reach the surface.

202   ● *Data from the Beaufort Gyre Experiment Project (BGEP)*

203   The BGEP has maintained an observing system in the Canadian Basin since 2003 and

204   provides in-situ observations over the Beaufort Gyre every summer. Although the BGEP has

205   maintained three bottom-tethered moorings since 2003, the shallowest depth of the

206   measured profiles for temperature and salinity is below 50 m. Hence, in this study, we only

207   use the Conductivity Temperature Depth (CTD) dataset from the cruise in 2016

208   (https://www2.whoi.edu/site/beaufortgyre/data/ctd-and-geochemistry/, last access: 14th

209   February 2022). SSS observations from these CTD profiles in the time period from 13th Sep

210   to 10th Oct 2016 are represented by the red triangles in Fig. 2.

211   ● *Data from Oceans Melting Greenland (OMG)*

212   The project Oceans Melting Greenland was funded by NASA to understand the role of the

213   ocean in melting Greenland's glaciers. Over a five-year campaign, this project collected

214   temperature and salinity profiles by Airborne eXpendable Conductivity Temperature Depth

215   (AXCTD) launched from an aircraft (*e.g.*, Fenty, et al, 2016). The deployed probe can sink to

216   a depth of 1000 meters, connected with a float by a wire. The measured temperature and

217   conductivity are then sent back to the aircraft. These salinity profiles collected during the first

218   OMG campaign in 2016 are downloaded from

219   https://podaac.jpl.nasa.gov/dataset/OMG_L2_AXCTD/ (last access: 10th February 2022). The

220   SSS from OMG distributed around Greenland, from 13th Sep to 10th Oct 2016 are shown as

221   the inverted blue triangles in Fig. 2.

222   ● *Data from the International Council for the Exploration of the Sea (ICES)*

223   Salinity profiles were also obtained from the ICES portal (https://www.ices.dk). Shown as

224   blue squares in Fig. 2, the locations of the profiles during the last 6 months of 2016 are

225   dense in the Nordic Seas and restricted to north of 58°N for this study. Valid salinity profiles

226   from ICES (last access: 9th February 2022) are obtained from 6th July to 23rd Nov in 2016.

227   ● *Data from other cruises at the Arctic Data Center (ADC)*

228   Surface salinity observations from scientific cruises are obtained from the Arctic Data

229   Center portal (https://arcticdata.io/catalog/data; last access: 17th Feb 2022). During the

230   model experiment, the first relevant cruise in ADC was SKQ201612S which was operated by

231   University of Alaska Fairbanks with the RV Sikuliaq. This cruise collected data from Nome,

232   Alaska on 3rd September, to the northeast Chukchi Sea, and then back to Nome at the end of

233   September 2016. The temperature and salinity profiles were collected by a Sea-Bird 911

234   CTD instrument package. All measurements at each station were done both down- and up-

235   cast ways. To produce water column profiles at each station, the down-cast data were

236   binned at 1 m intervals (Goñi et al.,2021). Besides the CTD profiles of SKQ201612S, more

237   seawater samples were collected via the surface underway system on the RV Sikuliaq.

238   Through a sea chest below the waterline (e.g., 4-8 m), the uncontaminated seawater was

239   pumped into the ship and the corresponding filtration system supplies samples every 3 hours

240   to the sensors (More details in Goñi et al., 2019). These SSS observations were obtained on

241   the 9th-27th of September, indicated as blue crosses in Fig. 2.

242   Moreover, SSS measurements were also collected from the Seabird CTD on board Sir

243   Wilfrid Laurier (SWL), but only in July 2016. This cruise is part of the annual monitoring from

244   the Canadian Coast Guard Service (Cooper et al., 2019). The SSS observations are

245   obtained near the Bering Strait close to the Pacific boundary of our model.

246   After filtering the diurnal signals by daily averages in observed surface salinity, all valid SSS

247   measurements from the above data sources are compared with the daily average SSS of the

248   three assimilation experiments listed in Table 1. The model data has been collocated with

249   the observations for validation. To estimate the forecast differences to observations, we use

250   the standard statistical moments:

251     $$Bias = \sum_{i=1}^{N} \sum_{1}^{O_i} (H\overline{\mathbf{X}}_i - \mathbf{y}_i) \ / \sum_{i=1}^{N} O_i \qquad (4),$$

252     $$MSD = \sqrt{\sum_{i=1}^{N} \sum_{1}^{O_i} (H\overline{\mathbf{X}}_i - \mathbf{y}_i)^2 \ / \sum_{i=1}^{N} O_i} \qquad (5),$$

253   Where i is the ith day, O_i represents the number of observations on this day, and N

254   represents the total number of days depending on the source of observations. Then $\overline{\mathbf{X}}_i$

255   represents the model daily average of the ensemble mean at the observation time. H is an

256   operator to extract the SSS simulation from the model at the observed location. The model

257   performance can then be quantitatively compared between the three assimilation runs.

258   In addition, we further introduce a two-sample Student's t-test to evaluate the significance of

259   the change of SSS bias in ExpV2/ExpV3 with respect to Exp0. Compared to in-situ

260   observations, the SSS misfits in Exp0 are the error array $\mathbf{e}_1$. The corresponding error array

261   from ExpV2 or ExpV3 is called $\mathbf{e_2}$. Thus, considering the null hypothesis H0: $\bar{\mathbf{e}}_1$ and $\bar{\mathbf{e}}_2$ are

262   the means of indiscernible random draws, the t-value can be calculated as follows:

263    $$t = \frac{|\bar{\mathbf{e}}_2 - \bar{\mathbf{e}}_1|}{\sqrt{s_1^2/(n_1 - 1) + s_2^2/(n_2 - 1)}}$$

264   Where $s_1(s_2)$ is the standard deviation in the $\mathbf{e_1}(\mathbf{e_2})$, and n_1 (n_2) is the number of observations.

265   For every t-value, the p-value from the above equation is the probability that random errors

266   would prove H0 wrong. Low p-values (<0.05) indicate that the change of bias due to

267   assimilation is significant.

268
269   **4. Results**

270   *4.1 Diagnosing using assimilation statistics*

271   The SSS innovations in the two assimilation runs of ExpV2 and ExpV3 are compared in Fig.

272   3, together with the number of assimilated SSS observations and the ensemble spread

273   calculated by the ensemble standard deviation. The total number of observations is at its

274   maximum in September when the sea ice cover is minimal. Since both versions of the SSS

275   product share the same time frequency (9-day average) and gridded format, the number of

276   assimilated observations in the two runs reached a maximum in the middle of September

277   (gray lines in Fig. 3). But the maximal number of SSS in ExpV3 shows higher than in ExpV2.

278   For ExpV2, the Root Mean Square (RMS) of the SSS innovation varies between 0.4 and 1.2

279   psu, but the mean of SSS innovation, calculated as the observation minus the model

280   simulation (cf. the bracket in Eq.1), shows a saline bias of 0.4 psu, highest in September.

281   However, in ExpV3 the salinity bias quickly disappears after a few data assimilation cycles.

282   The RMS of the SSS innovation is larger in ExpV3 between 0.6 and 1.6 psu, which can partly

283   be explained by the higher effective resolution of the V3.1 product and the double penalty

284   effect. In ExpV3, the RMS of the SSS innovation (the red line) jumps down after the first SSS

285   assimilation step. The RMS of SSS innovations and the observation errors both decrease

286   from summer to winter, following a seasonal cycle as the areas of fresher water get gradually

287   ice-covered. The domain-averaged observation errors are only slightly larger in ExpV3 than

288   in ExpV2, as explained above, and the RMS of SSS innovations becomes lower than the

289   observation errors near the end of the run, which indicates that the observation errors for the

290   V2.0 SSS have been overestimated.

291   In the top panels of Fig. 4, the SSS maps are shown for the control run (Exp0) in August and

292   September 2016, respectively. For Exp0 in August, low salinity waters are found in the

293   Beaufort Sea near the Mackenzie River and along the East Siberian coast. In September, the

294   fresher waters, below 30 psu, bridge the two areas in Exp0 probably due to sea ice melt,

295 although the lowest salinity near the Siberian coast remains unchanged from August to

296 September (as indicated by the 28 psu isoline). Compared with the SSS observations from

297 SMOS (Fig. 1), these two low-salinity waters are clearly underestimated in Exp0. Meanwhile,

298 the relatively saline 32 psu isoline crosses both the Eurasian basin and the Baffin Bay. In the

299 Laptev Sea, due to the significant effects of river runoff and ice melt, the salinity shows a

300 strong gradient from the southeast to the northern part. During winter, the salinity increases

301 to 34 psu, and decreases in summer near to 30 psu (Janout et al., 2017). In the northwest

302 Laptev Sea, the saline tongue of 32 psu extends eastward to the Taymyr Peninsula (TP).

303 North of the TP, the Kara Sea freshwater meets with the Atlantic Water pathways from the

304 Fram Strait and Barents Sea (shown in Figure 1 of Janout et al., 2017). Close to the TP, the

305 observations at the mooring profiles in Janout et al. (2017) show much fresher surface

306 salinity (29 psu) than the subsurface salinity (32 psu) in summer. Compared to the SMOS

307 SSS maps (shown in Fig. 1), only the V3.1 product shows the 32 psu isolines around the TP.

308 Another difference between the two SMOS products arises in the Chukchi Sea where the

309 V3.1 product is more saline than both the V2.0 product and SSS in Exp0.

310   The middle and bottom panels of Fig. 4 show the SSS differences in August and

311 September 2016 between the SSS assimilation runs and the control run. Figure 4c and 4d

312 both show a freshening of the coastal areas in the Kara Sea, Laptev Sea, and East Siberian

313 Sea, but in ExpV3 the freshening is stronger and wider (Fig. 4e and 4f). In the Beaufort Sea,

314 ExpV2 mainly brings a local freshening near the mouth of the Mackenzie River in August,

315 which then spreads out along the coast in September. The freshening in the BS brought by

316 ExpV3 affects a broader area, even including the Canadian Archipelago. ExpV3 also

317 freshens the SSS on both sides of Greenland Island. From August onwards, the SSS in

318 ExpV3 freshens by over 1 psu along the whole east Greenland coast, which clearly does not

319 happen in ExpV2. In fact, the 32 psu isoline in ExpV3 (not shown) extends hundreds of

320 kilometers further to the South East Greenland coast in comparison to Exp0 and ExpV2. The

321 rest of the Greenland coast is also fresher by 0.5 psu in ExpV3 during both months. This is a

322 sign of a consistent change in the V3.1 product.

323 Even though most of the SSS assimilation leads to a freshening of the surface, a few

324 locations show higher salinity than Exp0, these are different from ExpV2 to ExpV3. For

325 example, the saline increment near the Bering Strait is larger in ExpV3 in excess of 1 psu,

326 consistently with the difference between the two remote sensing products (Fig. 1).

327 Other increases in SSS concern small areas near estuaries and are more common in ExpV3.

328 The increase to the west of the Yamal Peninsula can be explained by a model setup bias in

329 the location of the Ob river but compensated by the SSS assimilation. In the above

330   comparisons of SSS maps, the central Arctic is not discussed, since the region is covered by
331   sea ice and the effect of assimilation is indirect.
332
333   *4.2 Comparison with independent in-situ observations*
334   Quality-checked in-situ observations in the Central Arctic are very unevenly distributed. After
335   pooling all platforms together, we further investigate the SSS misfits in six subregions of the
336   Arctic (Fig. 2 and Table 2). This section will present statistics of differences to independent
337   in-situ observations, separately considering marginal seas.
338
339   *Beaufort Sea (BS):* Figure 5 shows the scatterplots of SSS in the three runs against in-situ
340   observations from BGEP, OMG, and ICES. In the Beaufort Sea (top panel in Fig. 5), the
341   observed SSS varies in a range of 26-29 psu. The range of SSS in Exp0 is much smaller,
342   between 29-31 psu with a saline bias of 2.6 psu and an RMSD of 2.7 psu, but otherwise, it
343   shows a reasonably linear relationship (r=0.59). The SSS bias in Exp0 has the same value
344   as in Xie et al. (2019), although estimated using the BGEP observations in a different time
345   period (2011-2013). The range of SSS in ExpV2 is slightly improved to 28-30.5 psu. Further,
346   the bias is reduced by 0.5 psu, corresponding to bias and RMSD reductions of respectively
347   13.5% and 10.5% with respect to Exp0. In ExpV3, the SSS range is much closer, between
348   26.5 and 30.5 psu, and the resulting bias and RMSD reductions of SSS are respectively
349   26.3% and 17.3% with respect to Exp0. Both the bias reduction in ExpV2 and ExpV3 relative
350   to Exp0 pass the significance test ($\alpha = 0.05$) through Student's t-test. Furthermore,
351   compared to all in-situ SSS in BS (top panels in Fig. 7), the SSS misfits in ExpV3 show a
352   stronger reduction by 26.0% for bias and 20.6% for RMSD. ExpV2 reduces these errors by
353   half as much (13.5% for bias and 11.5% for RMSD). These results clearly indicate that the
354   new version of the SSS is more beneficial for data assimilation in the Beaufort Sea.
355
356   *Chukchi Sea (CS)*: Fig. 6 shows the SSS deviations as a function of time during the SKQ
357   cruise route. Figure 6a shows the surface levels from CTDs. The saline bias (2.8 psu) is
358   more pronounced than in the Beaufort Sea, which we attribute to the proximity to the model
359   boundary in the Bering Strait, relaxed to climatological values, where the interannual
360   variability of Pacific water is not included. After assimilating SSS products, a reduction of the
361   bias is observed during September, by 15.5% in ExpV2 and up to 22.2% in ExpV3. The
362   comparison to underway surface water samples (Fig. 6b) also shows an error reduction of
363   around 15%, though fewer differences between ExpV2 and ExpV3.
364   Considering other cruise data in the CS (Fig. 7; bottom panels), the SSS in Exp0 shows
365   almost uniform values with a saline bias of about 2.3 psu and an RMSD of 2.6 psu. A recent

366 observational study by Goñi et al. (2021) shows that the surface salinity of the CS during late
367 summer varies between 28-30 psu during the time period 2016-2017. The range of SSS
368 observations considered here is slightly broader (27-32 psu). The assimilation of SSS
369 products reduces the misfits (bias and RMSD). As in the BS, the SSS in ExpV3 has more
370 significant reductions in bias (17.7%) and RMSD (16.4%). After assimilation, the deviations
371 are in the same range as found in the BS. All the bias reductions in ExpV2 and ExpV3 are
372 significant compared to Exp0 through the t-test ($\alpha = 0.05$).
373
374 *Greenland Sea (GS)*: Most SSS observations around Greenland are from the OMG
375 programme, shown as the blue downward triangles in Fig. 2. Considering first all SSS
376 observations from OMG, the SSS misfits in the three runs (shown in the middle panels of Fig.
377 5) show smaller bias and RMSD than in the BS and the CS. However, the SSS in ExpV3 still
378 brings significant error reductions with a reduction of 32.6%/9.4% of the bias and RMSD
379 compared to Exp0. Notably, the SSS misfits in ExpV2 are almost identical to Exp0, which
380 indicates that the V2.0 SSS product was not informative there.
381 We now separate the evaluation in the East and West of Greenland covering the GS and
382 Baffin Bay (BB) areas as shown in Fig. 2 (also listed in Table 2). The top panel of Fig. 8
383 shows that all SSS observations available in the GS vary between 27 and 35 psu. This large
384 range includes fresh coastal waters, Arctic water, and Atlantic Water. The three assimilation
385 runs show different saline biases, especially for salinities lower than 30 psu. While in
386 observations the minimum salinity is below 28 psu, it only reaches 30 psu in ExpV3, and 31
387 psu in both Exp0 and ExpV2. As a result, the bias reduction in ExpV3 is over 50% and the
388 RMSD decreased by about 10.5% in the GS. ExpV2 is disappointingly similar to Exp0. This
389 is also the case in BB (shown in Fig. 8 bottom row), where differences between ExpV2 and
390 Exp0 are less than 0.02 psu. In contrast, ExpV3 reduces the SSS bias but does not
391 significantly reduce the RMSD in the BB. One possible explanation is the double-penalty
392 effect because the V3.1 product has a higher effective resolution than V2.0. This can be
393 seen in Fig. 8 as the ExpV3 values are more scattered.
394 Finally, we examine the SSS deviations in the Barents Sea and the Norwegian Sea. The
395 SSS bias and RMSD are the lowest in ExpV3 in Table 2, even though the reductions are not
396 as significant as in the area of fresher surface waters. Compared to the ICES observations
397 distributed in the North Atlantic and the Nordic Seas (blue squares in Fig. 2), the scatterplots
398 of Exp0 and ExpV2 are nearly identical (see the bottom panels in Fig. 5). The minimum
399 salinity in these two runs is 32 psu. The SSS bias and RMSD in both runs are also similar
400 (differences less than 0.01 psu). In contrast, lower salinity values are found in ExpV3, below
401 32 psu, although the saline bias remains around 0.5 psu on average. Notably, the SSS in

402 ExpV3 shows that data assimilation can reduce the bias by 15% compared to Exp0, but the

403 RMSD only reduced about 0.03 psu, also possibly due to the double penalty effect. This also

404 suggests that the improvements near the coast will be the next challenge for future versions

405 of the SSS product.

406

407 *4.3 Impact analysis of SSS assimilation*

408 The above section has demonstrated that the assimilation of remote sensing SSS generally

409 improves the match to independent in-situ measurements, although the improvements are

410 location-dependent. Since large areas are void of in-situ measurements, the increment for

411 other surface variables will also be interpreted for understanding the impacts incurred. The

412 increments are the differences between the analysis and the forecast. The calculation of

413 them is the result of the innovations of all assimilated observations multiplied by the Kalman

414 gain, as computed in Eq. (1). Since the DEnKF update is multivariate, we present the impact

415 of the assimilation on other model variables closely related to the SSS: SST and SIC. Since

416 the only difference in the setting between the three runs is the assimilation of SSS, we can

417 attribute the differences to the impact of SSS observations. In theory, if both the model and

418 observations were unbiased, the increments of other assimilated variables should generally

419 decrease because of the presence of a new SSS term in the denominator of the Kalman

420 Gain(The ensemble covariance matrices contain off-diagonal blocks of correlation between

421 SSS and dynamically related variables and so the assimilated observations usually compete

422 with each other). However, the SSS biases originating either from the model or observations

423 also affect the other model variables and increase the innovations on the following

424 assimilation step and thus the consecutive increments. Hypothetically, wherever the forecast

425 errors are caused by SSS errors, the increments of other variables should diminish. Figure 9

426 compares the time-averaged increments of SIC and seawater temperature in the top 3-m

427 layer (considered as SST here) in the three runs. The sign of the increments remains overall

428 the same across the three experiments, both for SST and SIC. The SST increments in the

429 three runs are negative in the open ocean and positive near the ice edge, as shown in the

430 right column of Fig. 9.

431 The SST increments in Exp0 and in ExpV2 are nearly identical, but in ExpV3 there are few

432 areas such as in the Kara Sea and in the Laptev Sea where the SST increments have been

433 suppressed. These are locations where the SSS and SST are positively correlated, so the

434 updated SSS by assimilation is also helpful in reducing the water temperature misfits near

435 the surface. The changes in SST are however small with respect to the large SSS

436 differences in Figure 4. In Exp0, the SIC increments are small (<5%) inside the ice pack. The

437 satellite SIC observations are assimilated every week and help to correctly position the ice

438 edge (Sakov et al., 2012). The increments exceed 5% along the ice edge, as can be seen in

439 the northern Barents Sea.

440 The assimilation of the V2.0 SSS product also shows minimal differences from Exp0 partly

441 because of the conservative sea ice mask in the V2.0 SMOS SSS. The SIC increments are

442 opposite to those of SST, showing that the assimilation warms the surface water where ice is

443 removed, which is consistent with Lisæter et al. (2003). Only minor differences between

444 ExpV2 and ExpV0 are visible along all areas swept by the ice edge during the 6-month

445 experiment, for example in the Kara Sea. In contrast, the assimilation of the V3.1 SSS

446 product shows larger changes in SIC increments than in ExpV2 with a broader area of

447 negative increments (removed ice) in the northern Barents Sea. This is not visibly related to

448 the SST increments but to the freshening caused by the assimilation of V3.1 SSS as SSS

449 and SIC are positively correlated in the northern Barents Sea, as shown by Fig. 2 in Sakov et

450 al. (2012). The increased SIC increments may be an indication that the SSS freshening could

451 be excessive.

452 Since the whole water column is updated by assimilation, the freshwater content is also

453 modified by the assimilation of SSS. There are however complex relationships between SSS

454 and FWC as shown by Fournier et al. (2020). The changes in FWC in the Arctic are

455 calculated as in Eq. (6) derived from Proshutinsky et al. (2009), although this method was

456 initially intended for the Beaufort Sea. Applying the same formula for interpolation of in-situ

457 observations, Proshutinsky et al. (2020) estimated the time-averaged summer freshwater

458 content in the Beaufort Gyre region in two time periods (1950-1980 and 2013-2018). In the

459 latter period, they located the FWC centre in the Beaufort Sea around (150°W, 75°N) and

460 drew the 20-m isoline over more than 5 degrees of latitude and nearly 30 degrees of

461 longitude on average. When compared to the earlier reference period, the FWC in the

462 Beaufort Sea has increased and its centre has shifted westward.

463 Following Proshutinsky et al. (2009), the model FWC in the Arctic is estimated as:

464 $$FWC = \int_{z_0}^{z_{ref}} (1 - \frac{S_{(z)}}{S_{ref}}) dz \tag{6}$$

465 Where the reference salinity value S_{ref} is taken at 34.8 psu, z_{ref} is the depth of the reference

466 salinity or the sea bed, and $S(z)$ is the salinity profile. Figure 10 shows the FWC on two

467 representative days, September 20th and October 20th, 2016. In Exp0, the reanalysis

468 reproduces the typical FWC distribution in the Arctic with a maximum in the Beaufort Sea.

469 The 20 m isolines in Fig. 10a and 10d show an increase in spatial coverage during October,

470 consistent with Rosenblum et al. (2021), but the 20 m isoline is not extending as far as 170°E

471 compared to Proshutinsky et al. (2020). After the assimilation of SSS products (either V2.0 or

472   V3.1), the amplitude and the spatial distribution of the FWC maximum increase slightly in the
473   Beaufort Sea (see Fig. 10b and 10c). A much larger increase of FWC appears on the East
474   Siberian shelf and in the coastal areas of the Laptev Sea and eastern Kara Sea, although to
475   a different extent in ExpV2 and in ExpV3. In the eastern Kara Sea, the FWC increases over a
476   wider area in ExpV2 than in ExpV3. To the west of the Yamal Peninsula, ExpV3 shows a
477   negative anomaly related to an incorrect location of the model river runoff, corrected in later
478   versions of the model. The SSS assimilation is able to correct the related fresh bias. In the
479   central Arctic, although the assimilated SSS measurements are masked by the sea ice
480   cover, the FWC differences north of 84°N are more pronounced in October than in
481   September, which indicates the advection of SSS increments by the Transpolar Drift Stream
482   (Rigor et al., 2002; Balibrea-Iniesta et al., 2018). These results suggest that the SSS
483   assimilation of both versions of SMOS satellite-based acts compensates for the insufficient
484   river summer runoff, redistributes the freshwater in the Arctic, and adjusts the freshwater
485   budget. However, because of the limited in-situ data, the above assessment remains
486   preliminary.
487   Further, we compare the daily time series of Arctic-averaged FWC from the three runs to the
488   north of 70°N (Fig. 11). The FWC increases in October-November to reach its maximum, and
489   gradually decreases thereafter. The impact of the week-long data assimilation cycles is
490   visible as instantaneous jumps on the three curves of the time series, but the assimilation of
491   SSS does not cause unrealistic imbalances. The FWC increases substantially due to SSS
492   assimilation, by about 25 cm. Notably, the assimilation of version 3.1 SSS causes a faster
493   increase during the first two months. Due to the absence of ground truth data in 2016, the
494   above comparison is not fully verified, but the timing of the peak is in better agreement with
495   the seasonal freshwater storage presented by the Ice-Tethered Profiler (ITP) data in Fig. 4a
496   of Rosenblum et al. (2021). In addition, we also notice that the amplitude of the seasonal
497   FWC seems too small in all experiments in Fig. 11, which can be related to insufficient thick
498   ice in TOPAZ (Uotila et al., 2019). More concrete evidence about the changed FWC will be
499   provided when the longer assimilation of the satellite-based SSS product is finished in the
500   near future.

501

502   **5.   Summary and discussions.**
503   The gridded SSS products from the SMOS satellite undoubtedly provide a way to constrain
504   errors in salinity, especially for an ocean reanalysis system. The present study is the first
505   observing system simulation experiment for the assimilation of SMOS SSS in the Arctic. In
506   this study, based on the TOPAZ reanalysis system, we compared a reanalysis assimilating

507 conventional observations with two new reanalysis runs which additionally assimilated two

508 versions of the SMOS SSS products from BEC.

509 After comparison with independent SSS observations from CTD and surface water samples

510 along cruise tracks, near-surface salinity errors have been significantly reduced compared to

511 the control experiment (Exp0). In the Beaufort Sea, the SSS bias and RMSD in ExpV3 are

512 reduced respectively by 26.0% and 20.6%. In ExpV2, the RMSD reduction is smaller (by

513 11.5%). In the Chukchi Sea, the reduction in SSS misfits in ExpV3 (bias:17.7%; RMSD:

514 16.4%) is also larger than in ExpV2 (bias: 15.5%; RMSD: 13.7%). Around Greenland, the

515 difference between the two products is even more pronounced, with a significant reduction in

516 the SSS bias (32.6%) and RMSD (9.4%) in ExpV3, while there is no notable improvement in

517 ExpV2. The difference is larger in the East Greenland Sea. The direct assimilation of SSS

518 from SMOS is more efficient at constraining the near-surface salinity than the multivariate

519 impact of other observations. This finding is also consistent with other SSS assimilation

520 experiments in the tropics (Chakraborty et al., 2015; Tranchant et al., 2019). Conversely,

521 when considering the multivariate impact of SSS on SIC (in Fig. 9) we find that the

522 assimilation of the V2 product does not affect the assimilation of sea ice concentrations while

523 the V3.1 product causes an increase in the negative increments, which could be an

524 indication of excessive freshening along the Siberian coast. In contrast, the increments of

525 SST in the open ocean are smaller in ExpV3, indicating a synergy effect of SST and SSS.

526 Overall, our data assimilation system did not detect obvious inconsistencies between the

527 SMOS SSS product and other assimilated observations.

528

529 Furthermore, this study shows error reductions of SSS when assimilating the V3.1 product

530 from SMOS even outside of the central Arctic in the Nordic Seas and along the Norwegian

531 coast. Moreover, our analysis shows how the spatial distribution of Arctic FWC changes as a

532 result of assimilating the two SMOS products. The time series of averaged FWC north of

533 70°N shows that the FWC in the whole central Arctic can be increased by about 25 cm using

534 DA. Our experiments show that the Arctic FWC can be redistributed horizontally after

535 assimilation, but the latter effect requires a longer assimilation run to be evaluated.

536 As a summary of the quantitative SSS comparisons (Table 2), the overall score of each

537 assimilation setup for each subregion can be defined by its ability to reduce the SSS bias

538 and RMSD by more than 9% relative to Exp0 (Fig. 2). The threshold value of 9% is not fully

539 arbitrary, referring to the reduction of SSS RMSD in GS, where the bias reduction is

540 significant (through the t-test). If both bias and RMSD meet this objective, we give a score of

541 1, but of 2 if only one of them is met. If neither of them exceeds 9%, the score is set to 3.

542 Thus outside of the central Arctic, the v2.0 SSS product loses its impact on the TOPAZ

543   system, but the V3.1 SSS brings significant impacts across the Arctic and further out, and

544   clearly benefits from its refined effective resolution (Martínez et al., 2022). Since there was

545   little evidence of a double-penalty effect in the validation RMSD apart from Baffin Bay, we

546   consider that the assimilation of the higher-resolution signals was efficient. However, the

547   assimilation did not improve the SSS significantly in the Barents Sea or other areas where

548   SSS gradients are weak. These may require higher accuracy to distinguish the Atlantic

549   waters from other water masses of salinity only slightly below 35 psu. To further improve the

550   SSS product, a combination with the Aquarius sensor using the same L-band frequency

551   (e.g., Lee et al, 2012), and SMAP (e.g., Tang et al., 2017; Reul et al., 2020) is desirable.

552

553   **Data availability.** All the in-situ observations for validation in this study are open access as

554   indicated in Sect. 3. The model results from Exp0 are the released TOPAZ reanalysis, which

555   is freely available from CMEMS (http://marine.copernicus.eu) or

556   https://doi.org/10.11582/2022.00043. The other assimilation experiments can be provided

557   freely upon personal communication.

558

559   **Author contributions**. JX initiated the design and carried out the assimilation

560   experiments. LB and RR contributed to the result interpretation. JM provided the SSS data.

561   CG and RC contributed to the uncertainty of the satellite data. All the authors contributed to

562   editing and correcting this paper.

563

564   **Competing interests.** The authors declare that they have no conflict of interest.

565

566   **Acknowledgments**:

567   Thanks to Yue Ying for the discussion. We are grateful to the in-situ data providers: the OMG

568   mission for the released final CTD data via https://podaac.jpl.nasa.gov/omg; the ICES data

569   portal (https://www.ices.dk); the Arctic Data Center (https://arcticdata.io/catalog/data); and

570   the BGEP data were available at the Woods Hole Oceanographic Institution

571   (https://www2.whoi.edu/site/beaufortgyre/) in collaboration with researchers from Fisheries

572   and Oceans Canada at the Institute of Ocean Sciences. This study has been supported by

573   the ESA Arctic+Salinity project and the following *CCN*, and also partly by the Norwegian

574   Research Council project (325242). The assimilation experiments and the plotting of the

575 results were performed on resources provided by Sigma2, the Norwegian Infrastructure for

576 High Performance Computing and Data Storage with the projects nn2293k and nn9481k and

577 the storage areas under the projects ns9481k and ns2993k.

578

579 **Reference:**

580 Balibrea-Iniesta, F., Xie, J., Garcia-Garrido, V., Bertino, L., Maria Mancho, A., and Wiggins,

581   S.: Lagrangian transport across the upper Arctic waters in the Canadian Basin. Q. J. Roy.

582   Meteor. Soc., 145(718), 76-91, doi:10.1002/qj.3404, 2018.

583 Argo: Argo float data and metadata from Global Data Assembly Centre (Argo GDAC).

584   SEANOE. doi:10.17882/42182, 2022.

585 Bertino, L., Ali, A., Carrasco, A., Lien, V., and Melsom, A.: THE ARCTIC MARINE FORECAST-

586   ING CENTER IN THE FIRST COPERNICUS PERIOD. 9th EuroGOOS International

587   conference, Shom; Ifremer; EuroGOOS AISBL, May 2021, Brest, France. pp.256-263. hal-

588   03334274v2. (Available from https://hal.archives-ouvertes.fr/hal-03334274v2/document)

589 Bouillon, S., Fichefet, T., Legat, V., and Madec, G.: The elastic-viscous-plastic method revised,

590   Ocean Modell., 7, 2–12, doi:10.1016/j.ocemod.2013.05.013, 2013.

591 Boutin, J., Jean-Luc, V., and Dmitry, K.: SMOS SSS L3 maps generated by CATDS CEC

592   LOCEAN, debias V3.0. SEANOE. 2018. Available online:

593   https://www.seanoe.org/data/00417/52804/.

594 Boutin J., Vergely J.-L., and Khvorostyanov D.: SMOS SSS L3 maps generated by CATDS

595   CEC LOCEAN. debias V7.0. SEANOE. doi:10.17882/52804#91742, 2022.

596 Boyer, T. P., Levitus, S., Antonov, J. I., Locarnini, R. A., and Garcia, H. E.: Linear trends in

597   salinity for the World Ocean, 1955–1998, *Geophys. Res. Lett.*, 32, L01604,

598   doi:10.1029/2004GL021791, 2005.

599 Carmack, E. C., Yamamoto Kawai, M., Haine, T. W. N., Bacon, S., Bluhm, B. A., Lique, C.,

600   Melling, H., Polyakov, I. V., Stra- neo, F., Timmermans, M.-L., and Williams, W. J.:

601   Freshwater and its role in the Arctic Marine System: Sources, disposition, storage, export,

602   and physical and biogeochemical consequences in the Arctic and global oceans, J.

603   Geophys. Res. Biogeo., 121, 675–717, doi:10.1002/2015JG003140, 2016.

604 Chakraborty, A., Sharma, R., Kumar, R., and Basu, S.: Joint Assimilation of Aquarius-derived

605   Sea Surface Salinity and AVHRR-derived Sea Surface Temperature in an Ocean General

606   Circulation Model Using SEEK Filter: Implication for Mixed Layer Depth and Barrier Layer

607   Thickness, J. Geophys. Res. Oceans, 120 (10), 6927-6942, doi:10.1002/2015JC010934,

608   2015.

609 Chassignet, E. P., Smith, L. T., and Halliwell, G. R.: North Atlantic Simulations with the Hybrid
610   Coordinate Ocean Model (HYCOM): Impact of the vertical coordinate choice, reference
611   pressure, and thermobaricity, J. Phys. Oceanogr., 33, 2504–2526, doi:10.1175/1520-
612   0485(2003)033>2504:NASWTH<2.0.CO:2, 2003.

613 Cooper, L. W., Grebmeier, J. M., Frey, K. E., and Vaglem, S.: Discrete water samples collected
614   from the Conductivity-Temperature-Depth rosette at specific depths, Northern Bering Sea
615   to Chukchi Sea, 2016. Arctic Data Center. doi:10.18739/A23B5W875, 2019.

616 Curry, R., Dickson, R., and Yashayaev, I.: A change in the freshwater balance of the Atlantic
617   Ocean over the past four decades, *Nature*, 426, 826–829, doi:10.1038/nature02206, 2003.

618 Dee, D. P., Uppala, S. M., Simmons, A. J., Berrisford, P., Poli, P., Kobayashi, S., Andrae, U.,
619   Balmaseda, M. A., Balsamo, G., Bauer, P., Bechtold, P., Beljaars, A. C. M., van de Berg,
620   L., Bid- lot, J., Bormann, N., Delsol, C., Dragani, R., Fuentes, M., Geer, A. J., Haimberger,
621   L., Healy, S. B., Hersbach, H., Hólm, E. V., Isaksen, L., Kållberg, P., Köhler, M., Matricardi,
622   M., McNally, A. P., Monge-Sanz, B. M., Morcrette, J.-J., Park, B.-K., Peubey, C., de Rosnay,
623   P., Tavolato, C., Thépaut, J.-N., and Vitart, F.: The ERA-Interim reanalysis:configuration
624   and performance of the data assimilation system, Q. J. Roy. Meteor. Soc., 137, 553– 597,
625   doi:10.1002/qj.828, 2011.

626 Dombrowsky, E., Bertino, L., Cummings, J., Brassington, G. B., Chassignet, E. P., Davidson,
627   F., Hurlburt, H. E., Kamachi, M., Lee, T., Martin, M. J., Mei, S., and Tonani, M.: GODAE
628   systems in operations. Oceanography, 22(3), 80–95, doi:10.5670/oceanog.2009.68, 2009

629 Drange, H. and Simonsen, K.: Formulation of air-sea fluxes in the ESOP2 version of MICOM,
630   Technical Report No. 125, Nansen Environmental and Remote Sensing Center, 23 pp.,
631   1996.

632 Fenty, I., Willis, J. K., Khazendar, A., Dinardo, S., Forsberg, R., Fukumori, I., Holland, D.,
633   Jakobsson, M., Moller, D., Morison, J., Meunchow, A., Rignot, E., Schodlock, M.,
634   Thompson, A.F., Tino, K., Rutherford, M., and Trenholm, N.: Oceans Melting Greenland:
635   Early results from NASA's ocean-ice mission in Greenland. Oceanography, 29(4):72-83,
636   doi:10.5670/oceanog.2016.100, 2016.

637 Font, J., Camps, A., Borges, A., Martín-Neira, M., Boutin, J., Reul, N., Kerr, Y. H., Hahne, A.,
638   and Mecklenburg, S.: SMOS: The challenging sea surface salinity measurement from
639   space, Proc. IEEE, 98(5), 649–665, doi:10.1109/JPROC.2009.2033096, 2010.Fournier, S.,
640   Lee, T., Wang, X., Armitage, T. W. K., Wang, O., Fukumori, I., and Kwok, R.: Sea Surface
641   Salinity as a Proxy for Arctic Ocean Freshwater Changes. Journal of Geophysical
642   Research: Oceans, 125(7). doi:10.1029/2020JC016110, 2020

643 Fujii, Y., Rémy, E., Zuo, H., Oke, P., Halliwell, G., Gasparin, F., et al.: Observing system
644   evaluation based on ocean data assimilation and prediction systems: on-going challenges

645   and a future vision for designing and supporting ocean observational networks. *Front. Mar.*

646   *Sci.,* 6(417), doi:10.3389/fmars.2019.00417, 2019.

647 Goñi, M. A., Corvi, E. R., Welch, K. A., Buktenica, M., Lebon, K., Alleau, Y., and Juranek, L.

648   W.: Particulate organic matter distributions in surface waters of the Pacific Arctic shelf

649   during the late summer and fall season. Marine Chemistry, 211, 75-93,

650   doi:10.1016/j.marchem.2019.03.010, 2019.

651 Goñi, M. A., Juranek, L. W., Sipler, R. E., and Welch, K. A.: Particulate organic matter

652   distributions in the water column of the Chukchi Sea during late summer. J. Geophys. Res.

653   Oceans, 126(9), doi:10.1029/2021JC017664, 2021.

654 Greiner, E., Verbrugge, N., Mulet, S., and Guinehut, S.: Quality information document for multi

655   observation global ocean 3D temperature salinity heights geostrophic currents and MLD

656   product, CMEMS-MOB-QUID-015-012, available at:

657   https://catalogue.marine.copernicus.eu/documents/QUID/CMEMS-MOB-QUID-015-

658   012.pdf (last access: 14 December 2022), 2021.

659 Janout, M. A., Hölemann, J., Timokhov, L., Gutjahr, O., and Heinemann, G.: Circulation in the

660   northwest Laptev Sea in the eastern Arctic Ocean: Crossroads between Siberian River

661   water, Atlantic water and polynya-formed dense water, J. Geophys. Res. Oceans, 122,

662   6630–6647, doi:10.1002/ 2017JC013159, 2017.

663 Johannessen, O. M., Shalina, E. V., and Miles, M. W.: Satellite evidence for an Arctic Sea ice

664   cover in transformation, *Science*, 286, 1937–1939, doi:10.1126/science.286.5446.1937,

665   1999.

666 Kaminski, T., Kauker, F., Eicken, H., and Karcher, M.: Exploring the utility of quantitative

667   network design in evaluating Arctic sea ice thickness sampling strategies. *The*

668   *Cryosphere*, 9(4), 1721–1733, doi:10.5194/tc-9-1721-2015, 2015

669 Kerr, Y. H., Waldteufel, P., Wigneron, J. P., Delwart, S., Cabot, F., Boutin, J., Escorihuela, M.

670   J., Font, J., Reul, N., Gruhier, C., Juglea, S., Drinkwater, M. R., Hahne, A., Martín-Neira,

671   M., and Mecklenburg, S.: The SMOS mission: New tool for monitoring key elements of the

672   global water cycle, Proc. IEEE, 98(5), 666–687, doi:10.1109/JPROC.2010.2043032,

673   2010.

674 Lee, T., Lagerloef, G., Gierach, M. M., Kao, H. -Y., Yueh, S. S., and Dohan, K.: Aquarius

675   reveals salinity structure of tropical instability waves. *Geophys. Res. Lett.*, 39, L12610,

676   doi:10.1029/2012GL052232, 2012.

677 Lisæter, K. A., Rosanova, J. and Evensen, G.: Assimilation of ice concentration in a coupled

678   ice-ocean model, using the Ensemble Kalman filter, Ocean Dyn., 53(4), 368–388,

679   doi:10.1007/s10236-003-0049-4, 2003.

Lu, Z., Cheng, L., Zhu, J., and Lin, R.: The complementary role of SMOS sea surface salinity observations for estimating global ocean salinity state, J. Geophys. Res. Oceans, 121, doi:10.1002/2015JC011480, 2016.

Martin, M. J., King, R. R., While, J., Aguiar, A. B.: Assimilating satellite sea-surface salinity data from SMOS, Aquarius and SMAP into a global ocean forecasting system. Q. J. Roy. Meteor. Soc., 145(719), 705-726, doi:10.1002/qj.3461, 2019.

Martínez, J., Gabarró, C., and Turiel, A.: Algorithm Theoretical Basis Document, Arctic+Salinity ITT, Tech. rep., BEC, Institut de Ciencies del Mar-CSIC, doi:10.13140/RG.2.2.12195. 58401, 2020.

Martínez, J., Gabarró, C., Turiel, A., González-Gambau, V., Umbert, M., Hoareau, N., González-Haro, C., Olmedo, E., Arias, M., Catany, R., Bertino, L., Raj, R. P., Xie, J., Sabia, R., and Fernández, D.: Improved BEC SMOS Arctic Sea Surface Salinity product v3.1, Earth Syst. Sci. Data, 14, 307–323, doi:10.5194/essd-14-307-2022, 2022.

Martín-Neira, M., Oliva, R., Corbella, I., Torres, F., Duffo, N., Durán, I., Kainulainen, J., Closa, J., Zurita, A., Cabot, F., Khazaal, A., Anterrieu, E., Barbosa, J., Lopes, G., Tenerelli, J., Díez-García, R., Fauste, J., Martín-Porqueras, F., González-Gambau, V., Turiel, A., Delwart, S., Crapolicchio, R., and Suess, M.: SMOS instrument performance and calibration after six years in orbit. Remote Sens. Environ., 180, doi:10.1016/j.rse.2016.02.036, 2016.

Mecklenburg, S., Drusch, M., Kerr, Y. H., Font, J., Martiìn-Neira, M., Delwart, S., Buenadicha, G., Reul, N., Daganzo-Eusebio, E., Oliva, R., and Crapolicchio, R.: ESA's soil moisture and ocean salinity mission: Mission performance and operations, IEEE TGARS, 50, 1354–1366, doi:10.1109/TGRS.2012.2187666, 2012.

Olmedo, E., Martínez, J., Turiel, A., Ballabrera-Poy, J., and Portabella, M.: Debiased non-Bayesian retrieval: A novel approach to SMOS Sea Surface Salinity, Remote Sens. Environ., 193, 103–126, doi:10.1016/j.rse.2017.02.023, 2017.

Olmedo, E., Gabarró, C., González-Gambau, V., Martínez, J., Ballabrera-Poy, J., Turiel, A., Portabella, M., Fournier, S., and Lee, T.: Seven Years of SMOS Sea Surface Salinity at High Latitudes: Variability in Arctic and Sub-Arctic Regions. *Remote Sensing*. 2018; 10(11):1772, doi:10.3390/rs10111772, 2018.

Proshutinsky, A., Krishfield, Timmermans, M.-L., Toole, J., Carmack, E., Mclaughlin, F., Williams, W. J., Zimmermann, S., Itoh, M., and Shimada, K.: Beaufort Gyre freshwater reservoir: State and variability from observations, J. Geophys. Res. Oceans, 114, 1–25, doi:10.1029/2008JC005104, 2009.

Proshutinsky, A., Krishfield, R., and Timmermans, M. -L.: Introduction to special collection on arctic ocean modeling and observational synthesis (FAMOS) 2: beaufort gyre phenomenon. *J. Geophys. Res. Oceans*, 125, e2019JC015400, doi:10.1029/2019JC015400, 2020.

716 Reul, N., Grodsky, S., Arias, M., Boutin, J., Catany, R., Chapron, B., D'Amico, F., Dinnat, E.,
717   Donlon, C., Fore, A., Fournier, S., Guimbard, S., Hasson, A., Kolodziejczyk, N., Lagerloef,
718   G., Lee, T., Le Vine, D., Lindstromn, E., Maes, C., Mecklenburg, S., Meissner, T., Olmedo,
719   E., Sabia, R., Tenerelli, J., Thouvenin- Masson, C., Turiel, A., Vergely, J., Vinogradova, N.,
720   Wentz, F., and Yueh, S.: Sea surface salinity estimates from spaceborne L-band
721   radiometers: An overview of the first decade of observation (2010–2019), *Remote Sens.*
722   *Environ.,* 242, 111769, doi:10.1016/j.rse.2020.111769, 2020.
723 Rigor, I. G., Wallace, J. M., and Colony, R. L.: Response of Sea Ice to the Arctic Oscillation,
724   *J. Climate*, 15, 2648, doi:10.1175/1520- 0442(2002)015<2648:ROSITT>2.0.CO;2, 2002.
725 Rosenblum, E., Fajber, R., Stroeve, J. C., Gille, S. T., Tremblay, L. B., and Carmack, E. C.:
726   Surface salinity under transitioning ice cover in the Canada Basin: Climate model biases
727   linked to vertical distribution of freshwater. Geophysical Research Letters, 48,
728   e2021GL094739, doi: 10.1029/2021GL094739, 2021
729 Sakov, P., Counillon, F., Bertino, L., Lisæter, K. A., Oke, P. R., and Korablev, A.: TOPAZ4: an
730   ocean-sea ice data assimilation system for the North Atlantic and Arctic, Ocean Sci., 8,
731   633–656, doi:10.5194/os-8-633-2012, 2012.
732 Solomon, A., Heuzé, C., Rabe, B., Bacon, S., Bertino, L., Heimbach, P., Inoue, J., Iovino, D.,
733   Mottram, R., Zhang, X., Aksenov, Y., McAdam, R., Nguyen, A., Raj, R. P., and Tang, H.:
734   Freshwater in the Arctic Ocean 2010–2019, Ocean Sci., 17, 1081–1102, doi:10.5194/os-
735   17-1081-2021, 2021.
736 Steele, M., Morley, R., and Ermold, W.: PHC: A global ocean hydrography with a high-quality
737   Arctic Ocean, J. Climate, 14, 2079–2087, doi: 10.1175/1520-0442(2001)014<2079:PAGOH
738   W>2.0.CO;2, 2001.
739 Storto, A., Alvera-Azcárate, A., Balmaseda, M. A., Barth, A., Chevallier, M., Counillon, F.,
740   Domingues, C. M., Drevillon, M., Drillet, Y., Forget, G., Garric, G., Haines, K., Hernandez,
741   F., Iovino, D., Jackson, L. C., Lellouche, J-M., Masina, S., Mayer, M., Oke, P. R., Penny, S.
742   G., Peterson, K. A., Yang, C. and Zuo, H.: Ocean Reanalyses: Recent Advances and
743   Unsolved Challenges. Front. Mar. Sci., 6(418), doi:10.3389/fmars.2019.00418, 2019.
744 Stroeve, J. and Notz, D.: Changing state of Arctic sea ice across all seasons, Environ. Res.
745   Lett., 13, 103001, https://doi.org/10.1088/1748-9326/aade56, 2018.
746 Stroh, J. N., Panteleev, G., Kirillov, S., Makhotin, M., and Shakhova, N.: Sea-surface
747   temperature and salinity product comparison against external in situ data in the Arctic
748   Ocean. J. Geophys. Res. Oceans, 120, 7223-7236, doi:10.1002/2015JC011005, 2015.
749 Supply, A., Boutin, J., Vergely, J. L., Kolodziejczyk, N., Reverdin, G., Reul, N., and Tarasenko,
750   A.: New insights into SMOS sea surface salinity retrievals in the Arctic Ocean. Remote
751   Sensing of Environment, 249, 112027, doi:10.1016/J.RSE.2020.112027, 2020.

Tang, W., Fore, A., Yueh, S., Lee, T., Hayashi, A., Sanchez-Franks, A., Martinez, J., King, B., and Baranowski, D.: Validating SMAP SSS with in situ measurements, Remote Sens. Environ., 200, 326–340, doi:10.1016/j.rse.2017.08.021, 2017.

Tranchant, B., Remy, E., Greiner, E., and Legalloudec, O.: Data assimilation of Soil Moisture and Ocean Salinity (SMOS) observations into the Mercator Ocean operational system: focus on the El Niño 2015 event, Ocean Sci., 15, 543–563, doi:10.5194/os-15-543-2019, 2019.

Uotila, P., Goosse, H., Haines, K., Chevallier, M., Barthélemy, A., Bricaud, C., Carton, J., Fuˇckar, N., Garric, G., Iovino, D., Kauker, F., Korhonen, M., Lien, V. S., Marnela, M., Massonnet, F., Mignac, D., Peterson, A., Sadikn, R., Shi, L., Tietsche, S., Toyoda, T., Xie, J., and Zhang, Z.: An assessment of ten ocean reanalyses in the polar regions, Clim. Dynam., 52, 1613–1650, doi:10.1007/s00382-018-4242-z, 2019.

Vinogradova, N. T., Ponte, R. M., Fukumori, I. and Wang, O.: Estimating satellite salinity errors for assimilation of Aquarius and SMOS data into climate models. J. Geophys. Res. Oceans, 119(8), 4732–4744, doi:10.1002/2014JC009906, 2014

Woodgate, R. A., Weingartner, T. J., and Lindsay, R.: Observed increases in Bering Strait oceanic fluxes from the Pacific to the Arctic from 2001 to 2011 and their impacts on the Arctic Ocean water column. Geophys. Res. Lett.,39, L24603, doi:10.1029/2012GL054092, 2012.

Xie, J., Bertino, L., Counillon, F., Lisæter, K. A., and Sakov, P.: Quality assessment of the TOPAZ4 reanalysis in the Arctic over the period 1991-2013. *Ocean Science*, **13**(1). doi: 10.5194/os-13-123-2017, 2017.

Xie, J., Counillon, F., and Bertino, L.: Impact of assimilating a merged sea-ice thickness from CryoSat-2 and SMOS in the Arctic reanalysis. *The Cryosphere*, **12**(11), 3671-3691. doi: 10.5194/tc-12-3671-2018, 2018.

Xie, J., Raj, R. P., Bertino, L., Samuelsen, A., and Wakamatsu, T.: Evaluation of Arctic Ocean surface salinities from the Soil Moisture and Ocean Salinity (SMOS) mission against a regional reanalysis and in situ data, Ocean Sci., 15, 1191–1206, doi:10.5194/os-15-1191-2019, 2019.

Yu, L.: A global relationship between the ocean water cycle and near-surface salinity, J. Geophys. Res., 116, C10025, doi:10.1029/2010JC006937, 2011.

Yu, L., Jin, X., Josey, S. A., Lee, T., Kumar, A., Wen, C., and Xue, Y.: The Global Ocean Water Cycle in Atmospheric Reanalysis, Satellite, and Ocean Salinity, *J. Climate*, **30**(10), 3829-3852, doi:10.1175/JCLI-D-16-0479.1, 2017

786 Yueh, S., West, R., Wilson, W., Li, F., Nghiem, S., and Rahmat- Samii, Y.: Error Sources and
787   Feasibility for Microwave Remote Sensing of Ocean Surface Salinity, IEEE T. Geosci.
788   Remote, 39, 1049–1059, doi: 10.1109/36.921423, 2001.
789 Zweng, M. M., Reagan, J. R., Antonov J. I., Locarnini, R. A., Mishonov, A. V., Boyer, T. P.,
790   Garcia, H. E., Baranova, O. K., Johnson, D. R., Seidov, D., and Biddle, M. M.: World Ocean
791   Atlas 2013, Volume 2: Salinity, Levitus, S. (Ed.), Mishonov, A., Technical Ed. NOAA Atlas
792   NESDIS 74, 39pp, doi:10.7289/V5251G4D, 2013.

Caption and figures:

Table 1. Settings of the three assimilation runs in 2016 with and without SSS.

	Assimilated obs.	Initial model states	End date of assimilation	SSS Observation Errors
Exp0	SST, SLA, T/S profile, SIC, SIT, and SID	6th July	28th Dec.	N/A
ExpV2	SSS V2.0 + obs. used in Exp0	6th July	28th Dec.	Eq. 3
ExpV3	SSS V3.1 + obs. used in Exp0	6th July	28th Dec.	Eq. 3

Table 2. Evaluation of SSS misfits (unit: psu) in the three assimilation runs according to the 6 areas indicated by the blue dashed lines in Fig. 2. The numbers in bold indicate the smallest misfit with a reduction of more than 9% relative to Exp0. The overall score depends on whether the bias and RMSD are reduced by at least 9%. If both criteria are met, the score equals 1, it is 2 if only one of them is met, and 3 otherwise. The start superscript means the bias changes passed the significance test using Student's t-test ($\alpha = 0.05$).

Areas in Fig. 2	Number of obs.	Bias (psu)			RMSD (psu)			Overall score	
		Exp 0	ExpV 2	ExpV 3	Exp 0	ExpV 2	ExpV 3	ExpV2	ExpV3
BS	98	2.81	2.43	***2.08***	2.87	2.54	***2.28***	1*	1*
CS	137	2.32	1.96	***1.91***	2.62	2.26	***2.19***	1*	1*
BSS	189	1.35	1.34	1.30	2.50	2.49	2.47	3	3
NS	669	0.43	0.44	***0.37***	1.19	1.19	1.16	3	2
GS	254	0.50	0.51	***0.24***	1.43	1.43	***1.28***	3	1*
BB	89	0.35	0.37	***0.12***	1.22	1.20	1.22	3	2
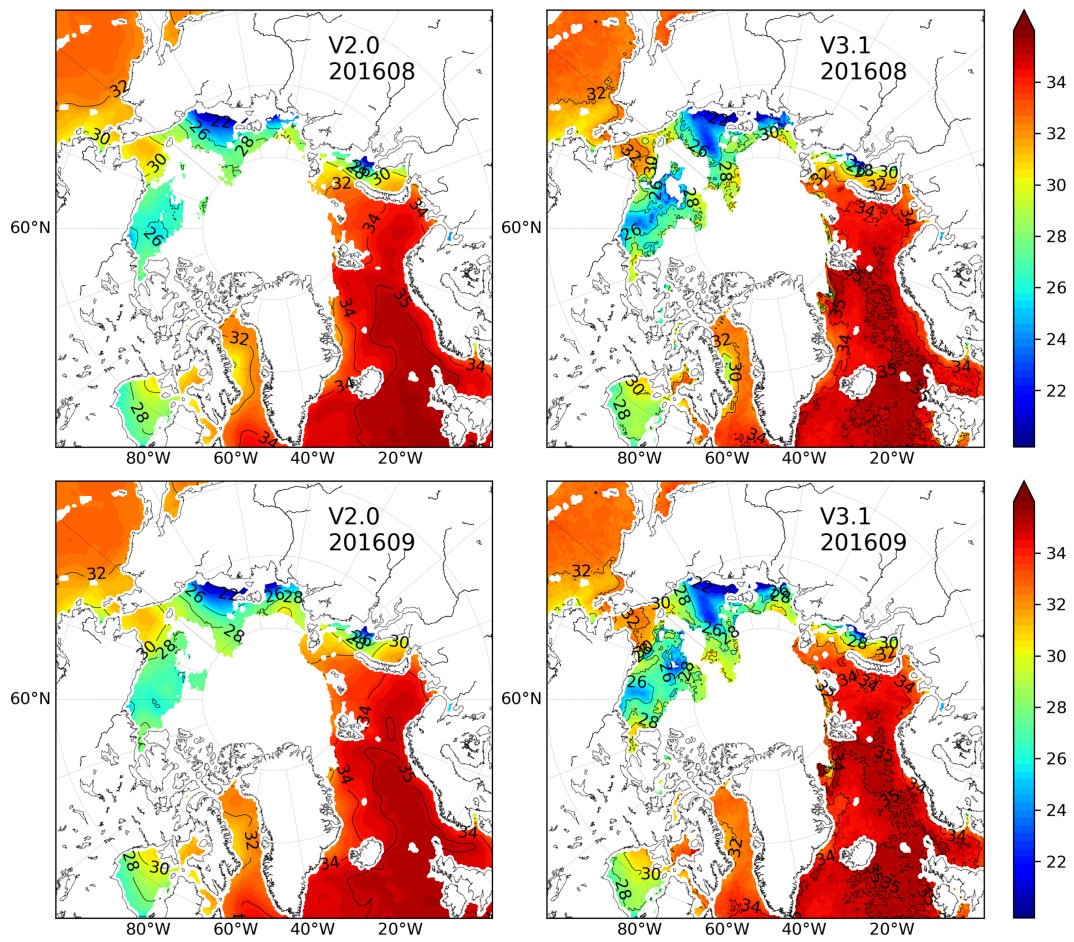
Fig. 1 Monthly SSS of Aug (top line) and Sep (bottom line) in 2016 from SMOS products of BEC V2.0 (left) and V3.1 (right). Note: the solid isolines of SSS are 22, 26, 28, 30, 32, 34, and 35 psu.
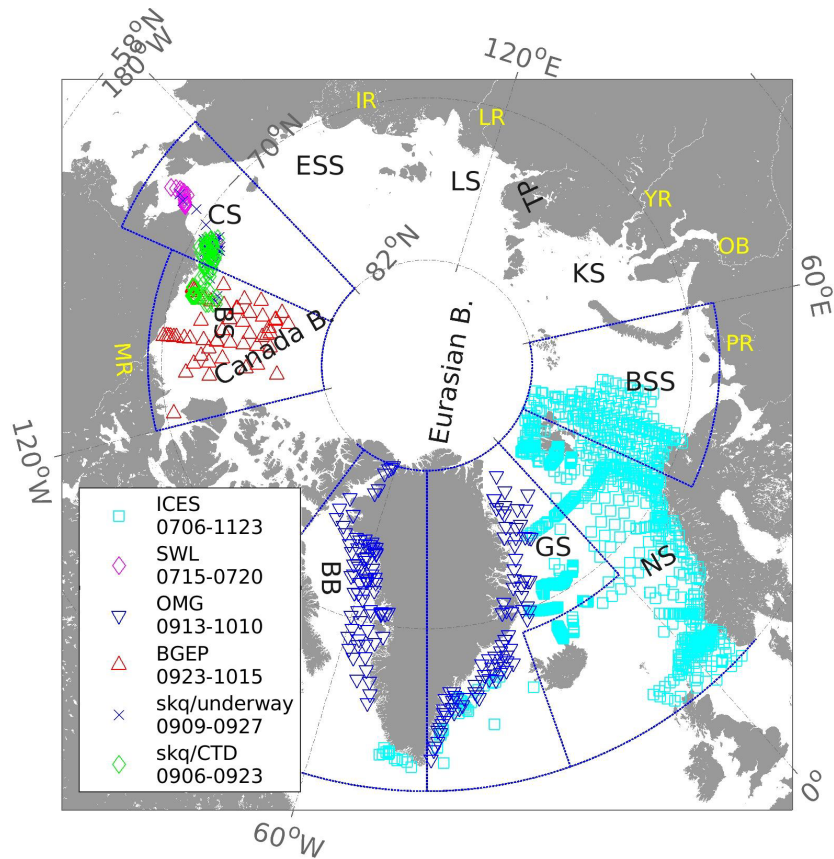
Fig. 2 Locations of the observed SSS from in-situ profiles and surface samples by cruises from July to December 2016. The marks note 6 observation sources, see the details in Section 2.3. The marginal seas delineated are the Beaufort Sea (BS), Chukchi Sea (CS), East Siberian Sea (ESS), Laptev Sea (LS), Kara Sea (KS), Barents Sea (BSS), Greenland Sea (GS), Norwegian Sea (NS), and Baffin Bay (BB). The main rivers around the Arctic region are the Mackenzie River (MR), Pechora (PR), the Ob (OB), Yenisey River (YR), Lena River (LR), and Indigirka River (IR). TP indicates the Taymyr Peninsula.
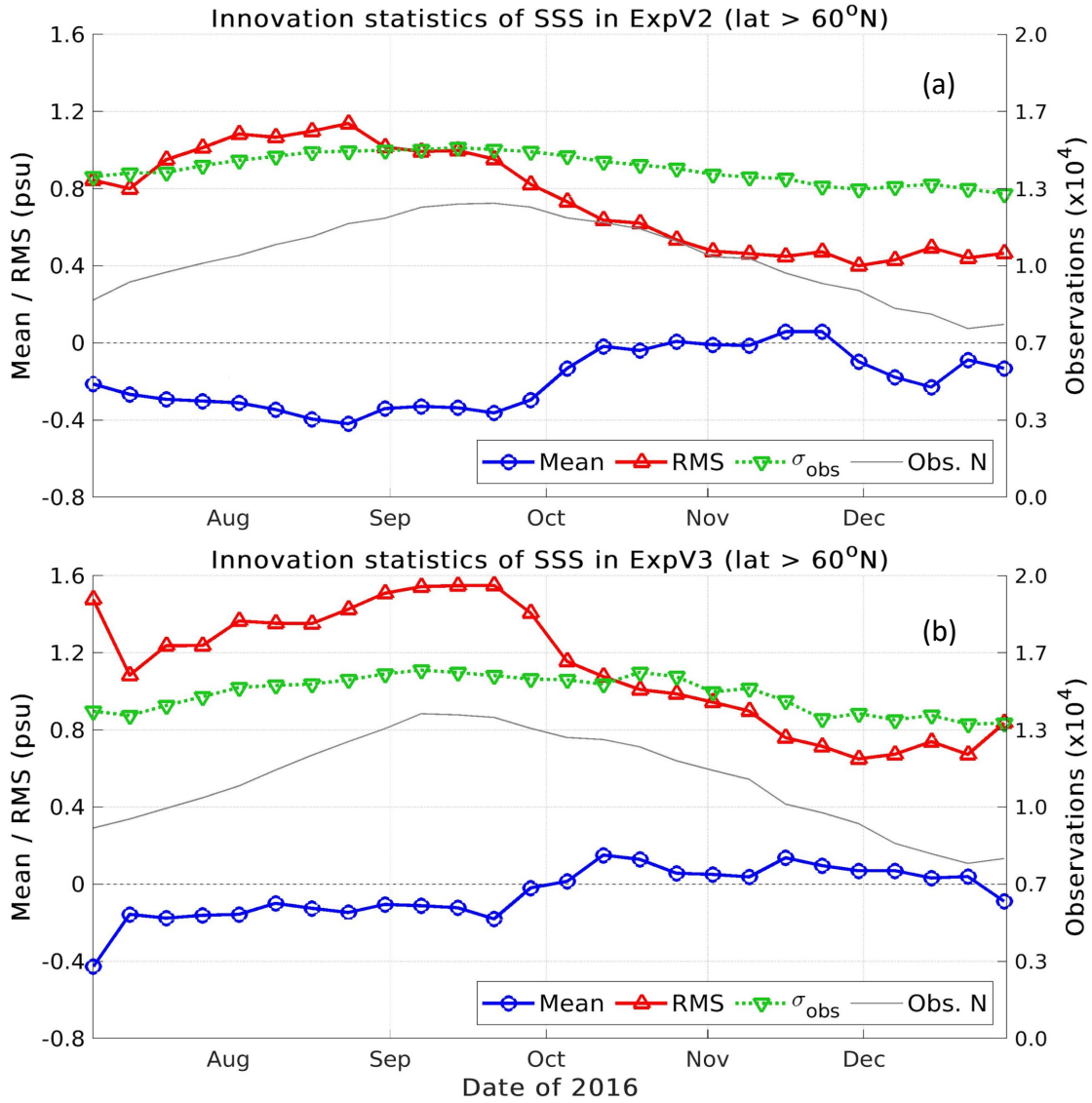
Fig. 3 Innovation statistics of SSS in the Arctic (>60ᵒN) from ExpV2 (a) and ExpV3 (b). The line with red triangles is the root mean squared innovation, and the blue dotted line shows the mean of innovations north of 60°N. The gray line represents the number of observations assimilated, and the green line with inverted triangles is the observation error standard deviation in the two runs.
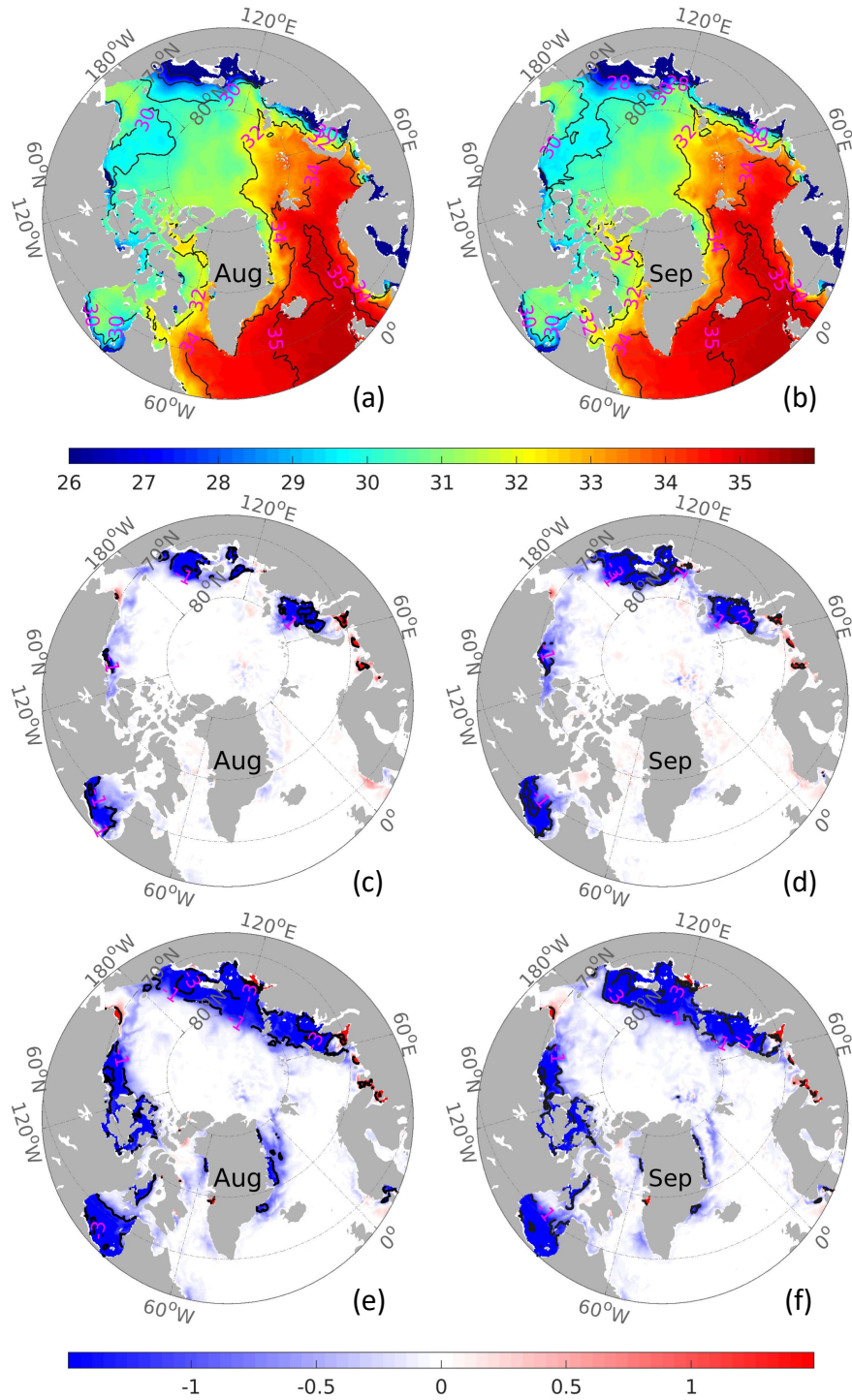
Fig. 4 **Top**: Monthly simulated SSS (unit: psu) from Exp0 in August (left column) and September 2016 (right column). The black isolines indicate the 26, 28, 30, 32, 34, and 35 psu, respectively. **Middle and bottom**: monthly SSS differences in ExpV2 (middle line) and ExpV3 (bottom line) with respect to Exp0. The black lines are -3, -1, 1, and 3 psu.
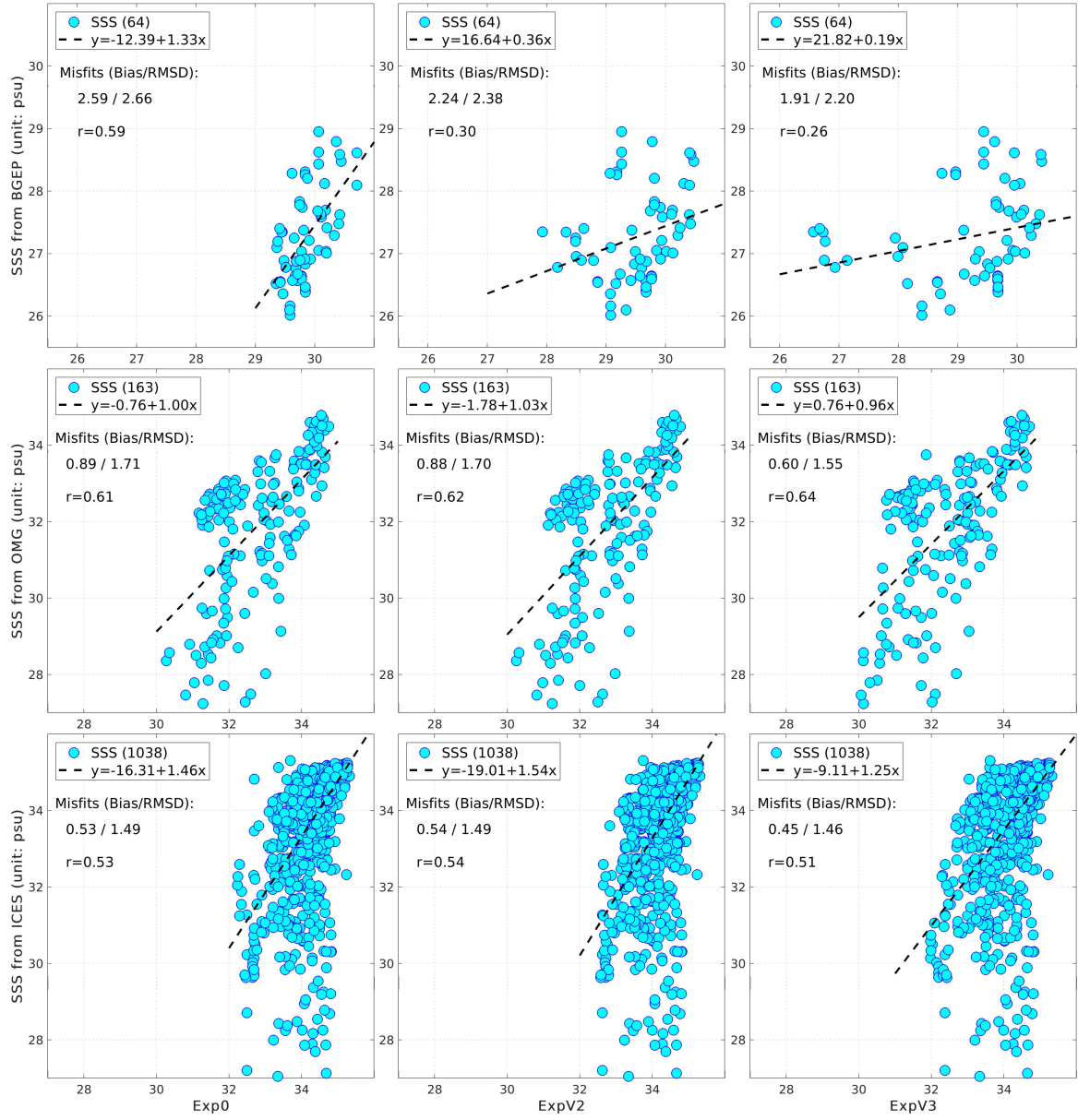
Fig. 5 Scatterplots of SSS in the TOPAZ assimilation runs against in-situ profiles (Top: from BGEP in the Beaufort Sea; Middle: from OMG in both Greenland Seas; Bottom: from ICES in the Nordic Seas as indicated in Fig.1 and descriptions in 2.1). The statistics of SSS misfits are indicated in each panel with the bias and the RMSD, respectively, the number of observations is given between parentheses. The dark dashed line represents the linear regression, and r is the linear correlation coefficient. All the correlation coefficients are over the 95% significance test.
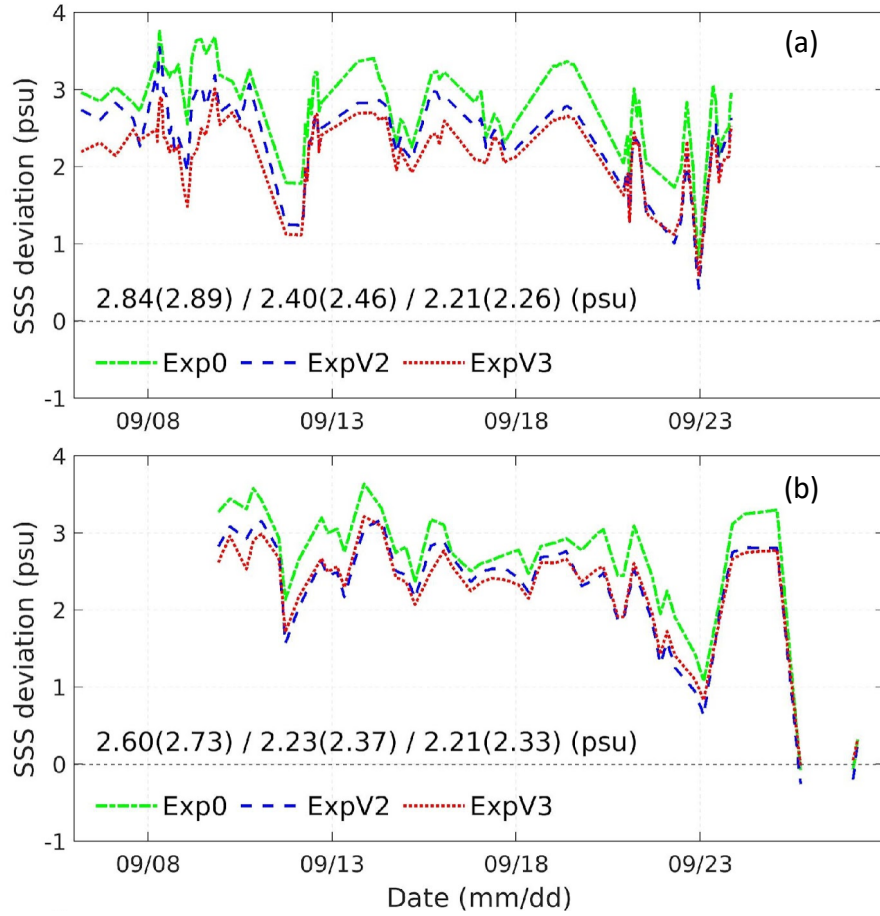
Fig. 6 Model-minus-observations SSS differences in the three assimilation runs against the SSS recorded in the Beaufort Sea and the Chukchi Sea along the SKQ cruise in 2016: a) from CTD profiles; b) from surface water samples underway in the same cruise. The biases are indicated in the same order as the legend from Exp0 to ExpV3, and the corresponding RMSD are inside parentheses.
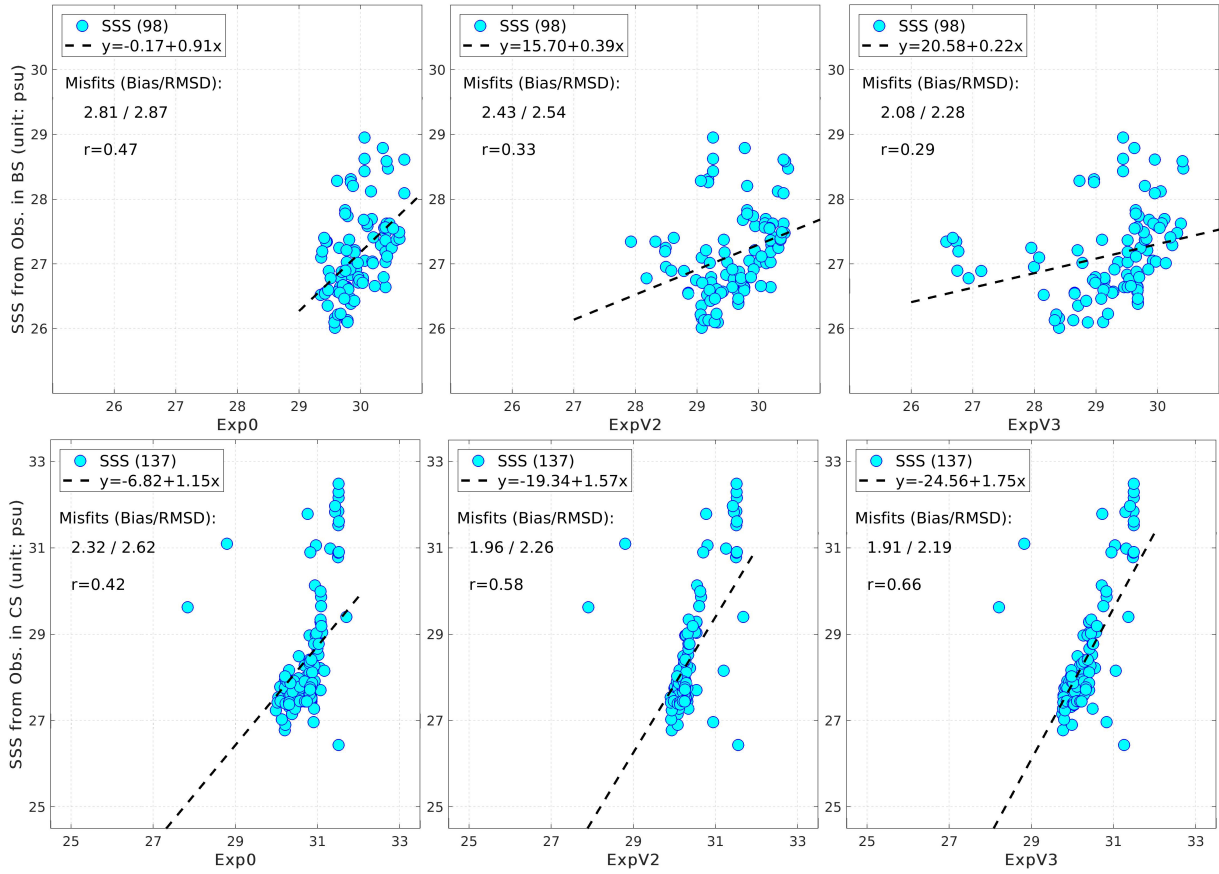
Fig. 7 Scatterplots of SSS (unit: psu) in the three assimilation runs Exp0, ExpV2, and ExpV3 against the CTD observations collected by different cruises in 2016. **Top**: Beaufort Sea; **Bottom**: Chukchi Sea as shown in Fig.1. All the correlation coefficients are over the 95% significance test.
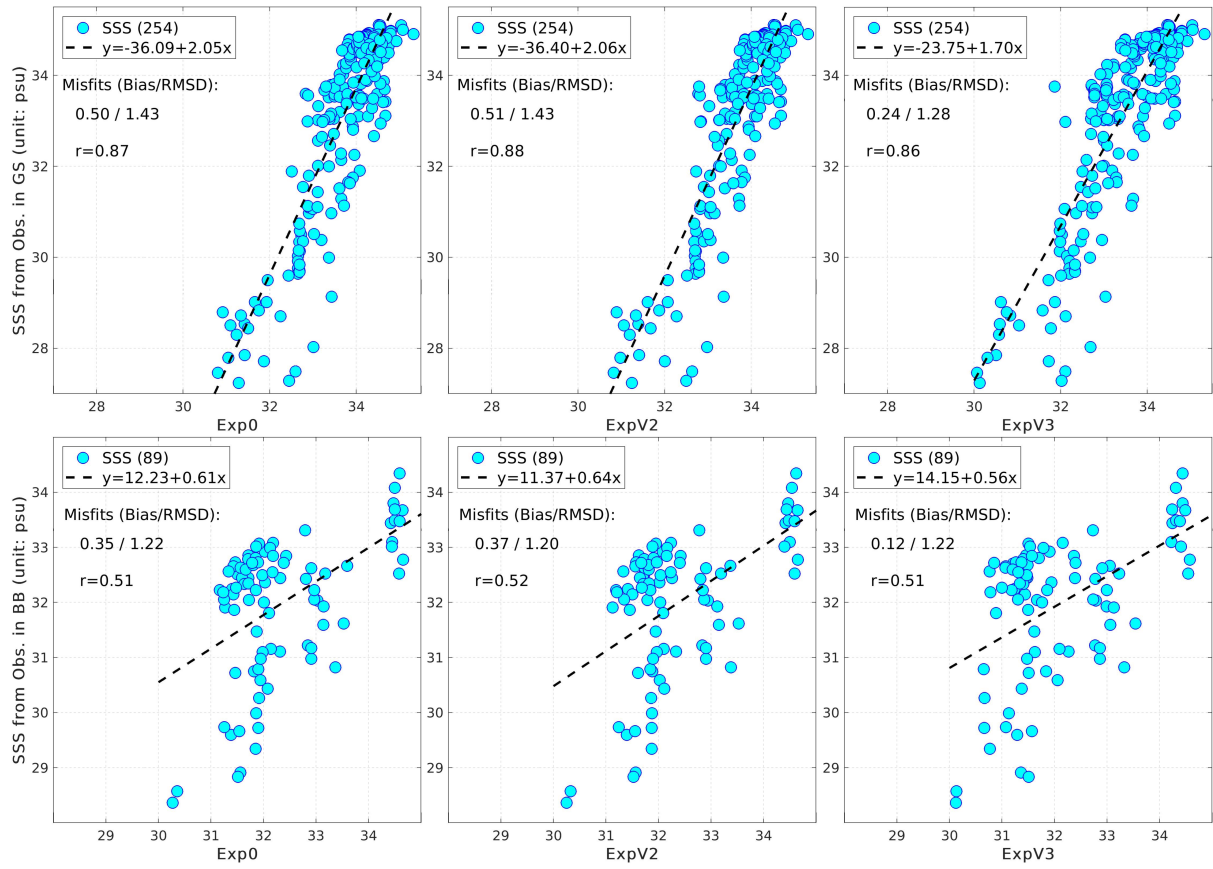
Fig. 8 Scatterplots of SSS (unit: psu) in the three assimilation runs Exp0, ExpV2, and ExpV3 against CTD observations from OMG and ICES in 2016. **Upper**: East Greenland Sea; **Bottom**: Baffin Bay as shown in Fig.1. The statistics of SSS misfits are indicated in each panel with the bias and the RMSD respectively, and the number of observations is given between parentheses. The dark dashed line represents the linear regression, and r is the linear correlation coefficient. All the correlation coefficients are over the 95% significance test.
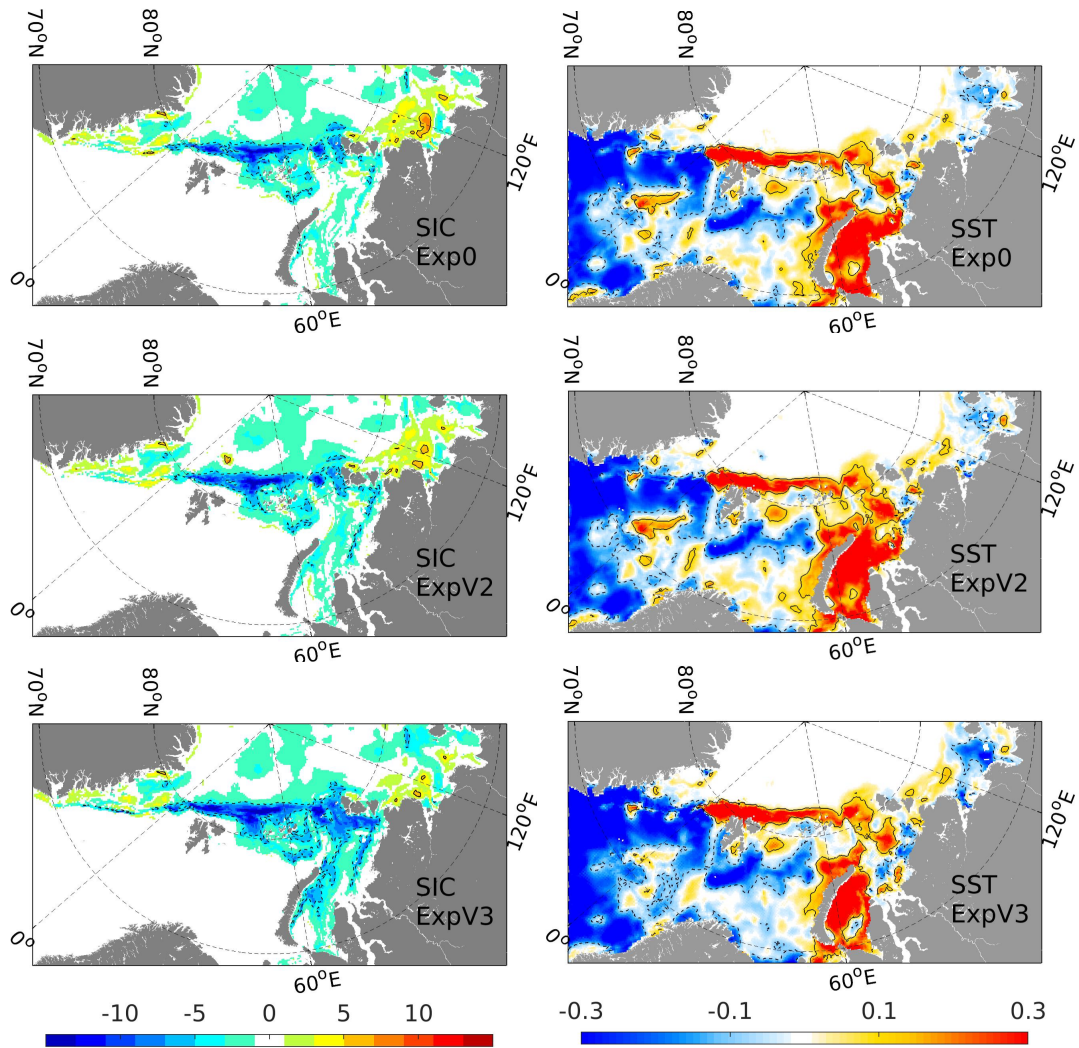
Fig 9. Mean of SIC and SST increments for the 6-months period (Top: in Exp0; Middle: in ExpV2; Bottom: in ExpV3). The figure shows the European Arctic for clarity. Left column: sea ice concentration (unit: %) with isolines of ± 5%. Right column: SST with isolines of ± 0.1°C.
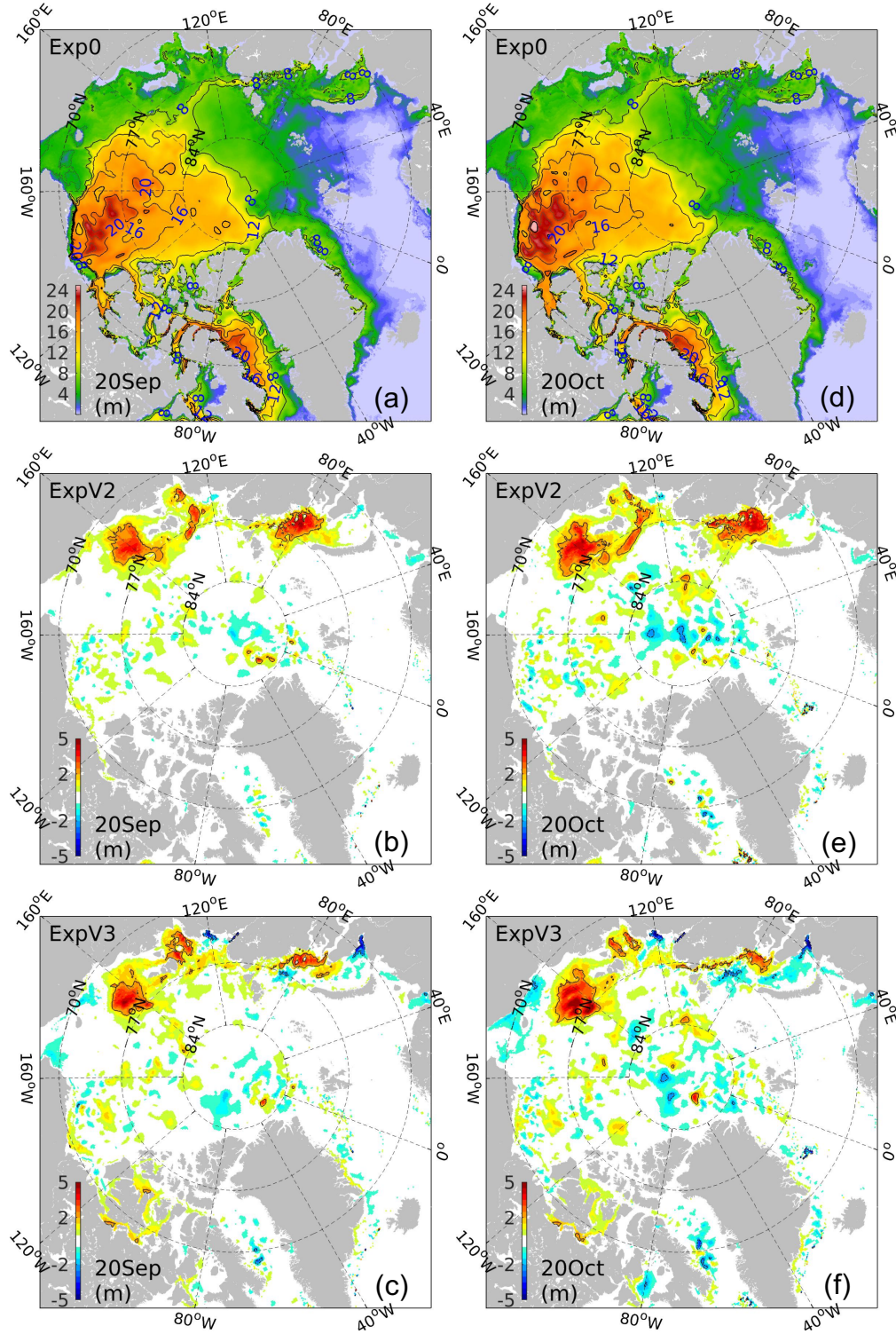
Fig. 10 Top: Freshwater contents (unit: m) on 20ᵗʰ September (left) and 20ᵗʰ October (right) 2016 in the Arctic Ocean from the three assimilation runs: Exp0. The interval of isolines is 4 meters. **Middle and bottom**: the FWC differences in ExpV2 (middle line) and ExpV3 (bottom line) concerning that in Exp0. The black lines indicate -2 m and 2 m differences.
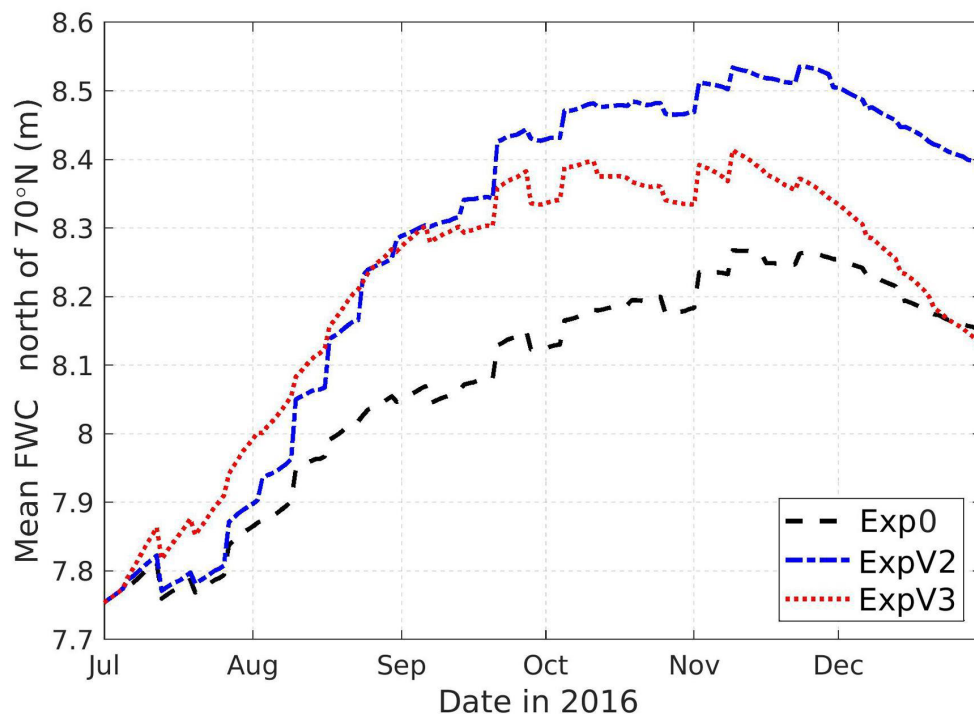
Fig 11. Arctic-wide means of freshwater content (unit: m) in the central Arctic (>70°N) from July to December 2016 for Exp0 (dark dashed), ExpV2 (blue dashed), and ExpV3 (red dotted).